How Do Secondary Minerals in Granite Help Distinguish Paleo-from Present-Day Permeable Fracture Zones? Joint Interpretation of SWIR Spectroscopy and Geophysical Logs in the Geothermal Wells of Northern Alsace

Carole Glaas, Jeanne Vidal, Patricia Patrier, Jean-François Girard, Daniel Beaufort, Sabine C. Petit, Albert Genter

▶ **To cite this version:**

Carole Glaas, Jeanne Vidal, Patricia Patrier, Jean-François Girard, Daniel Beaufort, et al.. How Do Secondary Minerals in Granite Help Distinguish Paleo-from Present-Day Permeable Fracture Zones? Joint Interpretation of SWIR Spectroscopy and Geophysical Logs in the Geothermal Wells of Northern Alsace. Geofluids, 2019, 2019, 10.1155/2019/8231816 . hal-02435169

HAL Id: hal-02435169
https://cnrs.hal.science/hal-02435169

Submitted on 10 Jan 2020

HAL is a multi-disciplinary open access archive for the deposit and dissemination of scientific research documents, whether they are published or not. The documents may come from teaching and research institutions in France or abroad, or from public or private research centers.

L'archive ouverte pluridisciplinaire **HAL**, est destinée au dépôt et à la diffusion de documents scientifiques de niveau recherche, publiés ou non, émanant des établissements d'enseignement et de recherche français ou étrangers, des laboratoires publics ou privés.

Hindawi
Geofluids
Volume 2019, Article ID 8231816, 20 pages
https://doi.org/10.1155/2019/8231816

Research Article

How Do Secondary Minerals in Granite Help Distinguish Paleo- from Present-Day Permeable Fracture Zones? Joint Interpretation of SWIR Spectroscopy and Geophysical Logs in the Geothermal Wells of Northern Alsace

Carole Glaas,[1,2,3] **Jeanne Vidal**,[2,4] **Patricia Patrier**,[3] **Jean-François Girard**,[1] **Daniel Beaufort**,[3] **Sabine Petit**,[3] **and Albert Genter**[2]

[1]*UMR 7516 IPGS, University of Strasbourg, CNRS, 5 Rue René Descartes, 67084 Strasbourg Cedex, France*
[2]*ES-Géothermie, Bat Le Belem 5 Rue de Lisbonne, 67300 Schiltigheim, France*
[3]*UMR 7285 IC2MP, HydrASA, University of Poitiers, CNRS, Bat B8 Rue Albert Turpain, TSA51106, F-86073 Poitiers Cedex 9, France*
[4]*FCFM, Department of Geology, Andean Geothermal Center of Excellence (CEGA), University of Chile, Plaza Ercilla 803, Santiago, Chile*

Correspondence should be addressed to Carole Glaas; carole.glaas@es.fr

Received 17 May 2019; Revised 11 September 2019; Accepted 24 September 2019; Published 11 December 2019

Guest Editor: Tanguy Robert

Copyright © 2019 Carole Glaas et al. This is an open access article distributed under the Creative Commons Attribution License, which permits unrestricted use, distribution, and reproduction in any medium, provided the original work is properly cited.

The investigation of permeable hydrothermally altered and fractured zones and their distribution is a key issue for the understanding of fluid circulation in granitic rocks, on which the success of geothermal projects relies. Based on the use of short-wave infrared (SWIR) spectroscopy applied to rock cuttings coupled with interpretation of geophysical logs, we propose an investigation of the clay signature of fault and fracture zones (FZ) inside the granitic basement. This methodology was applied to two geothermal wells: GRT-2 from the Rittershoffen and GPK-1 from the Soultz-sous-Forêts (Soultz) geothermal sites, both located in the Upper Rhine Graben (URG). A total of 1430 SWIR spectra were acquired and analysed. Variations in the 2200 nm absorption band area are correlated with hydrothermal alteration grades. The 2200 nm absorption band area is found to reflect the illite quantity and its variations in the granitic basement. Low, stable values are observed in the unaltered granite facies, showing good reproducibility of the method, whereas scattered high values are associated with high hydrothermal alteration and FZs. Variations in the 2200 nm absorption band area were correlated with the gamma ray and electrical resistivity logs. This procedure allowed us to confirm that illite mainly controls the resistivity response except inside the permeable FZs, where the resistivity response is controlled by the geothermal brine. Thus, the architecture of these permeable FZs was described precisely by using a combination of the 2200 nm absorption band area data and the electrical resistivity log. Moreover, by correlation with other geophysical logs (temperature (T), porosity, and density), paleo-permeable and currently permeable FZs inside the reservoir were distinguished. The correlation of SWIR spectroscopy with electrical resistivity logs appears to be a robust tool for geothermal exploration in granitic reservoirs in the URG.

1. Introduction

The mid-Carboniferous granitic basement of the Upper Rhine Graben (URG) has been affected by several extensional and compressional tectonic phases that developed a multi-scale fracture network during the Tertiary [1, 2]. Today, the network hosts hydrothermal circulations and acts as the main pathway through which the natural brine sustains wide convection cells [3–5]. More than 30 years of geothermal research in the pilot geothermal project of Soultz-sous-Forêts (Soultz) (Alsace, France) led to a 3D knowledge of those multiscale fault and fracture networks [6, 7]. Fault and fracture networks will be designated by the general term "FZ" in this paper. Their internal complexity in terms of

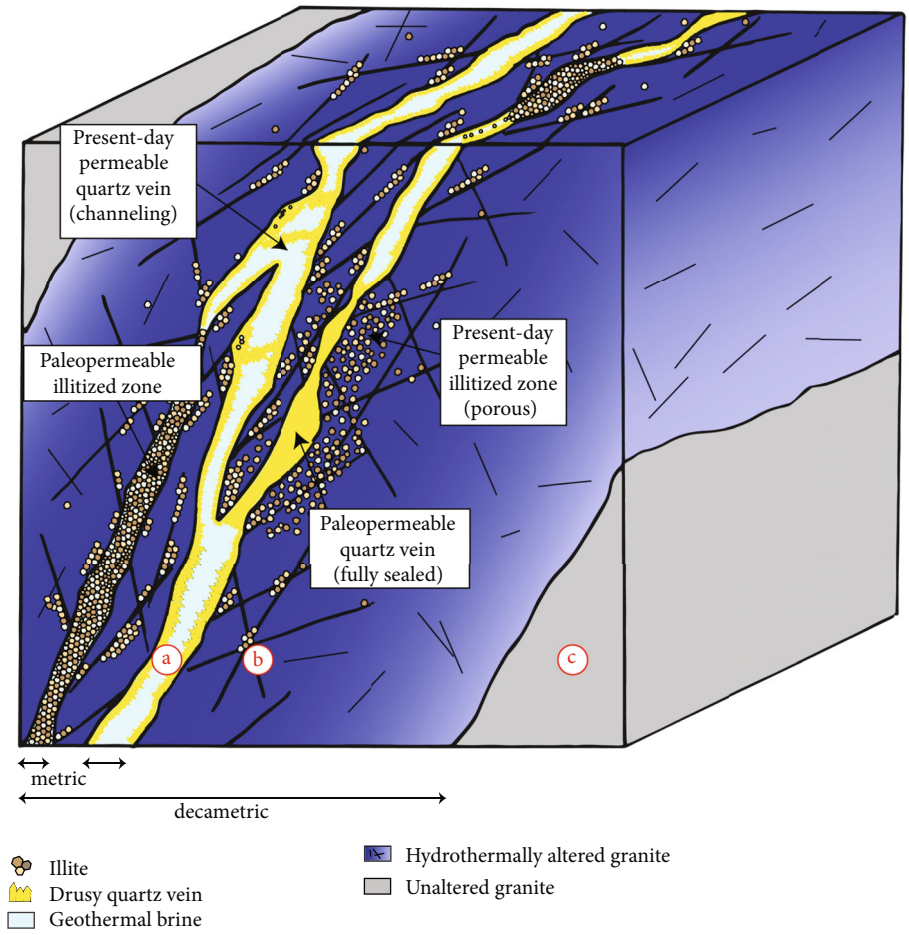

Figure 1: Complexity of a FZ after Caine et al. [71]. We can differentiate three zones: (a) the fault core, which can be a pathway for fluid if illite and quartz veins are not totally sealing the zone, (b) the damage zone, which can be sealed or opened with fractures that are acting as fluid pathways, and (c) the unaltered granite, which shows generally very low permeability.

architecture and associated permeability is a key question that must be answered when granitic rocks are used as hydrogeological reservoirs, for nuclear waste disposal, or as deep geothermal systems (Figure 1) [4, 8–12]. In the URG, the current targets for geothermal projects are hydrothermal fractured reservoirs in granitic rocks lying under a thick sedimentary cover [13]. Benefitting from lessons learned during the Soultz project and gained on several deep geothermal wells in Northern Alsace, we decided to avoid drilling subvertical wells in nearly vertical fracture systems to maximize the intersection of permeable FZs. Accordingly, a new drilling approach consisting of targeting deviated well trajectories crosscutting highly dipped FZs in the granitic basement was developed. However, these FZs can act either as permeable conduits and as paleo-permeable barriers for natural fluid transport (Figure 1). Therefore, due to primary mineral dissolution and/or secondary mineral precipitation related to fluid-rock interaction, the resulting permeability of FZs can increase or even decrease, increasing the challenge of obtaining successful geothermal wells [14–18].

This paper aims to develop a method to both characterize the hydrothermal alteration and evaluate the degree of permeability of the granitic reservoir intersected by geothermal wells in the context of the URG. Hydrothermal alteration of the buried granitic basement in the URG wells is systematically expressed by an illitization process [6, 7, 13, 19, 20]. Routinely used for the mining industry, short-wave infrared (SWIR) spectroscopy is an innovative method for geothermal systems [21]. Here, SWIR spectroscopy was used to detect illitic minerals (illite and illite-rich illite/smectite mixed layers) in the studied geothermal wells. However, the use of SWIR spectroscopy alone does not permit differentiation of whether this high illitization is the clay signature of permeable FZs contributing to the well's productivity or injectivity, or a signature of paleo-permeable FZs that are now sealed by secondary minerals. To distinguish paleo-permeable from currently permeable FZs, we propose an innovative method based on the correlation between SWIR signature, geophysical logs (T, gases, porosity, density, gamma ray, and electrical resistivity), and cuttings observations.

After describing the SWIR method and the several geophysical logs used in this study, the SWIR results will be presented for two geothermal wells drilled in Rittershoffen (GRT-2) and Soultz (GPK-1), respectively, and the specific

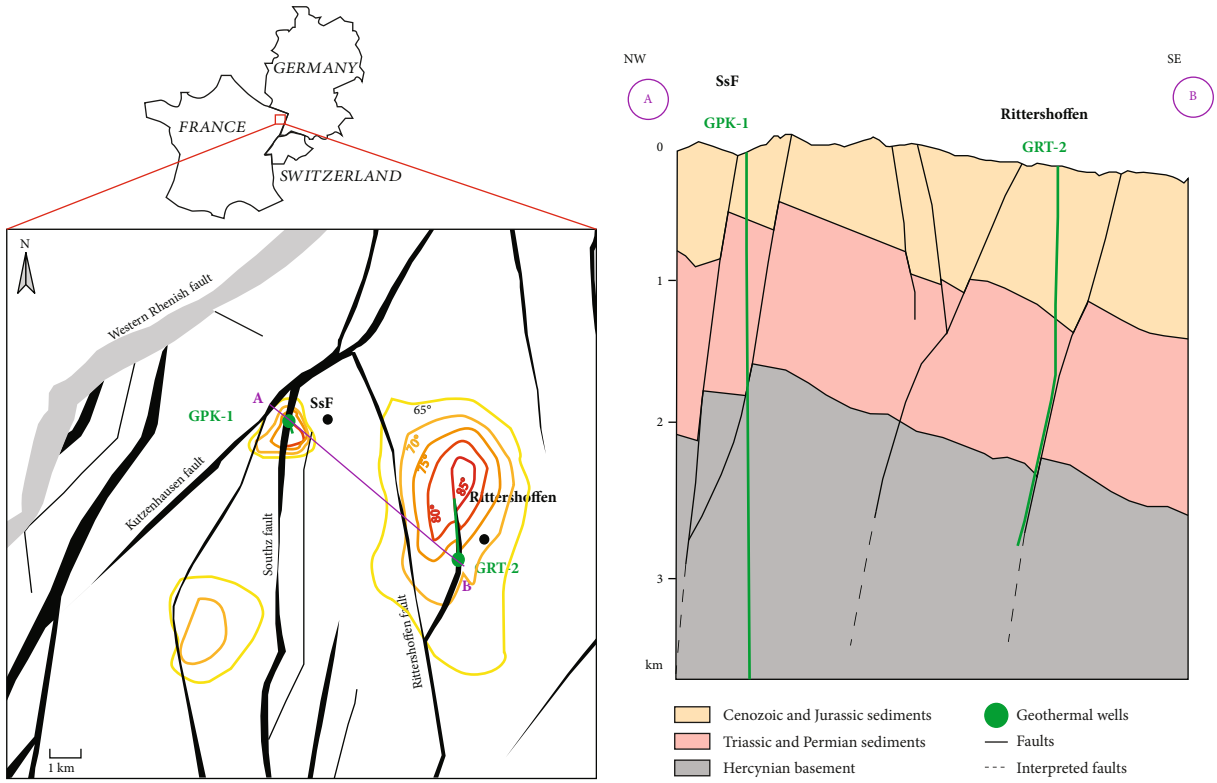

Figure 2: (a) Structural map of the top of the granitic basement from the GeOrg geoportal with the well trajectories (green), the thermal anomalies [3], and the Soultz (SsF) and Rittershoffen localizations. (b) Geological cross section through the GPK-1 and GRT-2 wells crossing the URG sedimentary cover and granitic basement; the well trajectory of the GRT-2 well is a NW-SE projection on the cross section, from the last 3D seismic campaign [72].

signatures and architectures of the FZs will be detailed. In the next step, the geophysical logs and SWIR results will be correlated and used to differentiate paleo- and present-day permeable zones. Finally, we will discuss the applicability of the SWIR method and its implications for the understanding of the mineralogy and the distribution of illitization at the well scale.

2. Geological Setting

2.1. Soultz and Rittershoffen Sites. In 2019, two deep geothermal plants exploiting deep fractured granite are operating in France. These plants produce a total of 24 MWth for industrial use at Rittershoffen and 1.7 MWe for the electrical grid at Soultz. Both sites are located in the URG approximately 40 km north of Strasbourg and target the hydrothermally altered granitic basement as a geothermal reservoir (Figure 2(a)).

The Soultz GPK-1 well was drilled vertically from 0 to approximately 2000 m measured depth (MD) in 1987 and was then deepened almost vertically to 3590 m MD in 1992 (Figure 2(b)). It crosses the Cenozoic and Mesozoic sedimentary covers before reaching the top of the Paleozoic granitic basement at 1376 m MD. The drilling of this well in 1987 was conducted according to an old geothermal concept, involving the creation of an artificial heat exchanger by hydraulic stimulation created by vertical wells [22–25]. The well was hydraulically stimulated several times to enhance the connection between the well and the reservoir [26, 27]. The FZs in the granitic basement are mainly oriented N160-170°E and subvertical, and most of them dip more steeply than 65° eastward or westward [14]. On drilling, natural very saline brines were encountered in fractured and altered zones bearing secondary minerals of hydrothermal origin [28]. Five main permeable FZs ranging from 20 to 40 m in apparent thickness are intersected at 1645, 1814, 2000, 2818, and 3495 m MD. In 2004, the Soultz site was composed of five deep wells that in fact revealed numerous permeable FZs [28].

The Rittershoffen project was initiated in 2008, and its target was the Rittershoffen normal fault, which is crossed by two deep wells, GRT-1 and GRT-2. The production well GRT-2 was drilled subvertically from 0 to 2480 m MD crossing the sedimentary cover to the top basement and was highly deviated (40° to the north) down to 3196 m MD crossing the granitic basement (Figure 2(b)). The target was to crosscut the main local fault as long as possible. This normal fault, which is located approximately 15 km east of the western Rhenish border fault, is oriented N5°E based on subsurface geological data [29, 30]. The GRT-2 well is therefore slightly deviated but tangent to the local fault over its approximately 400 m apparent length (Figure 2(b)). The GRT-2 well

revealed a high productivity index of 4 L/s/bar without any stimulation; thus, a hydrothermal concept could be implemented [13, 31]. Achieved in 2016, this Rittershoffen project proved to be a great success, with an operational plant producing a flow rate of 70 L/s at surface T of 168°C [32]. In the granitic section of the open hole of the GRT-2 well, four main permeable FZs ranging from 15 to 40 m in apparent thickness were intersected at 2533, 2770, 2950, and 3052 m MD [31, 33, 34].

Observations conducted on continuous and high-quality coring of the EPS-1 well from Soultz highlighted a multiscale fracture network [35]. Small-scale fractures with no evidence of displacement are filled with carbonates, chlorite, iron oxides, epidote, and sulphides, and faults visible at the core scale are filled with drusy quartz (euhedral quartz crystals as coatings on or infillings in fractures), carbonates, barite, and clay minerals. In the case of the Rittershoffen wells, for which no core was available, only the largest faults could be identified (small-scale fractures were hardly identified) because only cuttings and acoustic image logs were available.

2.2. Alterations of the Granitic Basement. During the cooling of the crystalline pluton, the granite underwent a pervasive alteration that presents the petrographic and mineralogical features of the propylitic facies. Today, it exhibits several grades of hydrothermal alteration that are also related to fluid circulation [36, 37]. The unaltered crystalline granitic basement at Rittershoffen and Soultz is composed of primary muscovite, biotite, K-feldspar, plagioclase, and quartz [37, 38]. This primary mineralogy is affected by hydrothermal alteration, and specific mineralogical associations reflect the various alteration grades encountered. According to previous studies of the Soultz geothermal wells, the hydrothermal alteration grades in the granite are well known from core observations [16, 17, 37, 39–41]. In this study, the core mineralogy and hydrothermal alteration grades were crossreferenced with the minerals observed in the cuttings using a binocular magnifier, although the texture information and the mineral assemblage were not reflected in the cuttings (Figure 3). The mineralogy of the cuttings was determined through a semiquantitative approach using a three-class scale [18, 33]. The hydrothermal alteration grades—low (HLOW), moderate (HMOD), high (HHIG), and extreme (HEXT)—are described in Figure 3 [42–46]. The granitic facies identified in the cuttings include two types of granite, "unaltered" granite (GRAN), affected by a propylitic alteration related to the cooling of the pluton [14, 47], and the presence of locally reddish granite (RED), containing a large number of red K-feldspar megacrysts that have been oxidized through intense exposure to weathering fluids. The presence of illite in the granitic basement as a major signature of hydrothermal alteration was confirmed by complementary laboratory analyses. In previous studies of the GRT-2 well, X-ray diffraction (XRD) was performed on the <5 μm fraction of selected cuttings; in this way, three groups of illitic minerals (well-crystallized illite, poorly crystallized illite, and illite-rich illite/smectite mixed layers) were identified [18]. The chemical compositions of the clay minerals were obtained using a scanning electron microscope (SEM) coupled with energy-dispersive X-ray spectroscopy (EDS). This study showed that permeable FZs were associated with the occurrence of poorly crystallized illite and illite/smectite mixed layers that crystallized during hydrothermal circulation [18]. XRD measurements of the GPK-1 well's cuttings were also performed in this study; the results showed the presence of illite in fractured and altered zones as well as the presence of chlorite and biotite in HLOW and GRAN.

3. Materials and Methods

3.1. SWIR Spectroscopy Method

3.1.1. Materials. The cuttings (chip samples) collected during the drilling of the wells were first washed using sieves and then dried on-site in an oven at 80°C for 40 minutes, by the mud logger unit. In the case of the GRT-2 well, the cuttings were sampled every 3 m in depth in the studied 8 1/2″ drilled section. Thus, one bag of cuttings represents approximately 0.1 m^3 of rock. For the GPK-1 well, the cuttings were sampled every 1 m in depth; thus in the 9 5/8″ drilled section from 1400 to 2850 m MD, one bag of cuttings represents approximately 0.04 m^3 of rock, and in the 7 5/8″ drilled section from 2850 to 3590 m MD, one bag of cuttings represents approximately 0.025 m^3 of rock. The sampling included in this study encompasses all the facies described in the foregoing section (Figure 3). The average grain size of the cuttings chips in each sample varies between 0.5 and 2 mm. The chip size can be highly influenced by drilling tool wear. For this reason and because the chip size of the cuttings influences the SWIR intensity (the higher the chip size, the higher the SWIR intensity), the changes of drilling tool are also presented in this work.

3.1.2. Measurement Conditions. The SWIR spectral domain extends from 1000 to 2500 nm. If the wavelength of the infrared radiation is close to the vibrational energy of the eigenmode of the molecule, it causes vibration of some bonds and the infrared radiation energy is absorbed. This is conveyed by absorption bands on the infrared spectrum acquired at the corresponding wavelength in the midinfrared (MIR) domain. In the SWIR domain, we can observe the harmonics and the combinations of these absorption bands [48]. In total, 240 cuttings samples from the GRT-2 well and 1190 cuttings samples from the GPK-1 well were analysed. The SWIR measurements were performed at the same time for each well; thus, the acquisition conditions (hygrometry of the room, ambient temperature) are homogeneous for each well. Because very few expandable clay minerals are present in the granite, even when it has been hydrothermally altered, the SWIR data are not very sensitive to the hygrometry parameter. This is confirmed by the reproducibility of the low values of the 2200 nm absorption band area in the unaltered granite for all the geothermal wells studied in the URG. The spectrometer used is a TerraSpec 4 Standard Res Mineral Analyzer created by Analytical Spectral Devices, Inc. (Malvern PANalytical company) equipped with two SWIR

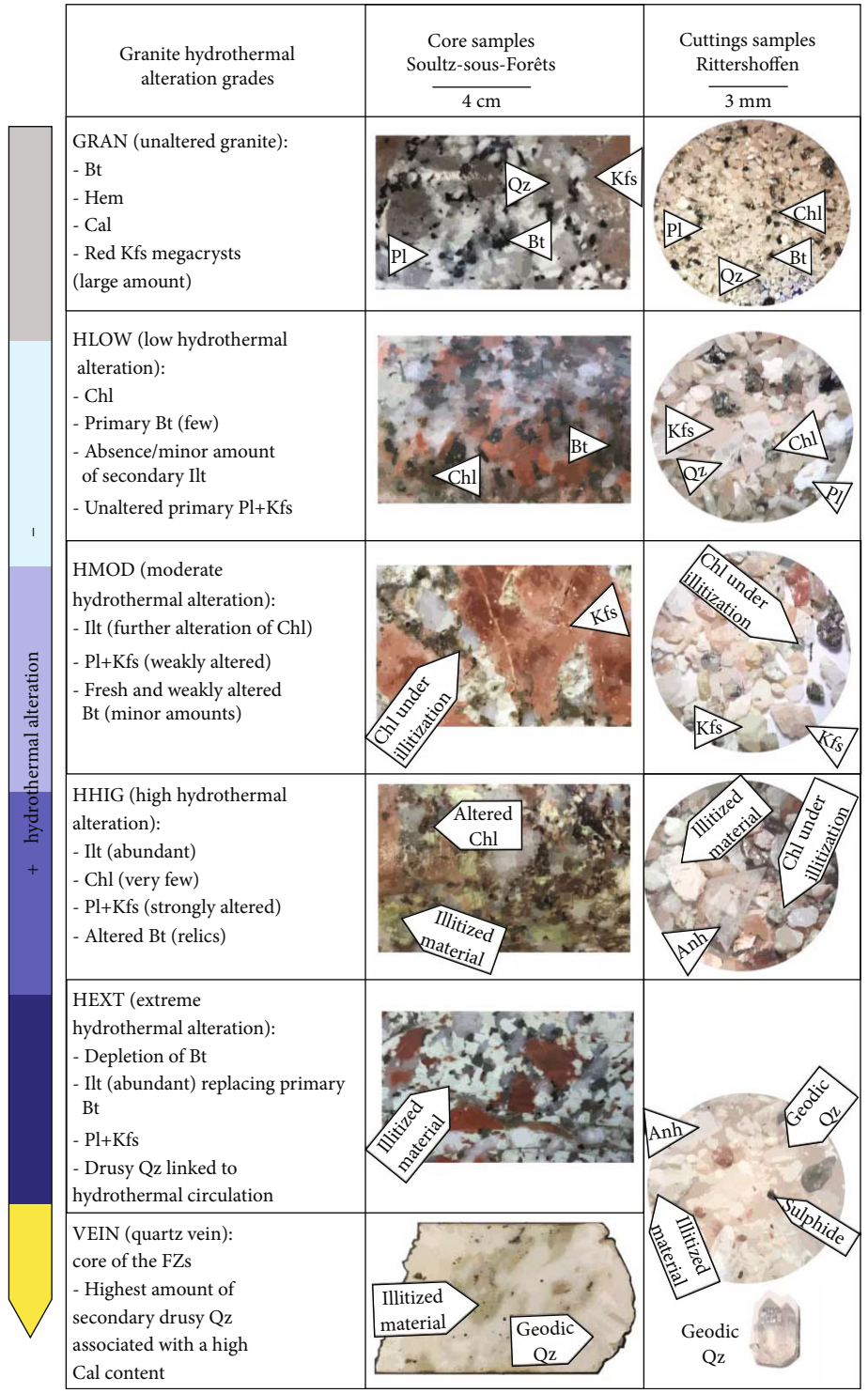

Figure 3: Examples of mineralogical assemblages of the granitic basement observed in cores (middle) and in cuttings (right); these assemblages define the different hydrothermal alteration grades (left). GRAN: unaltered granite; HLOW: low hydrothermal alteration; HMOD: moderate hydrothermal alteration; HHIG: high hydrothermal alteration; HEXT: extreme hydrothermal alteration; VEIN: secondary drusy quartz vein; Anh: anhydrite; Bt: biotite; Cal: calcite; Chl: chlorite; Hem: hematite; Ilt: illite; Kfs: potassic feldspars; Pl: plagioclase; Qz: quartz.

detectors. The spectral domain from 350 to 2500 nm is covered at a spectral resolution of 3 nm from 350 to 1000 nm and at a spectral resolution of 10 nm from 1000 to 2100 nm. The scanning time of 100 milliseconds made it possible to conduct the measurements rapidly for all granitic sections. The wavelength reproducibility is 0.1 nm with an accuracy of 0.5 nm. The reproducibility of the measurement was tested by measuring the same sample five times; this resulted in a

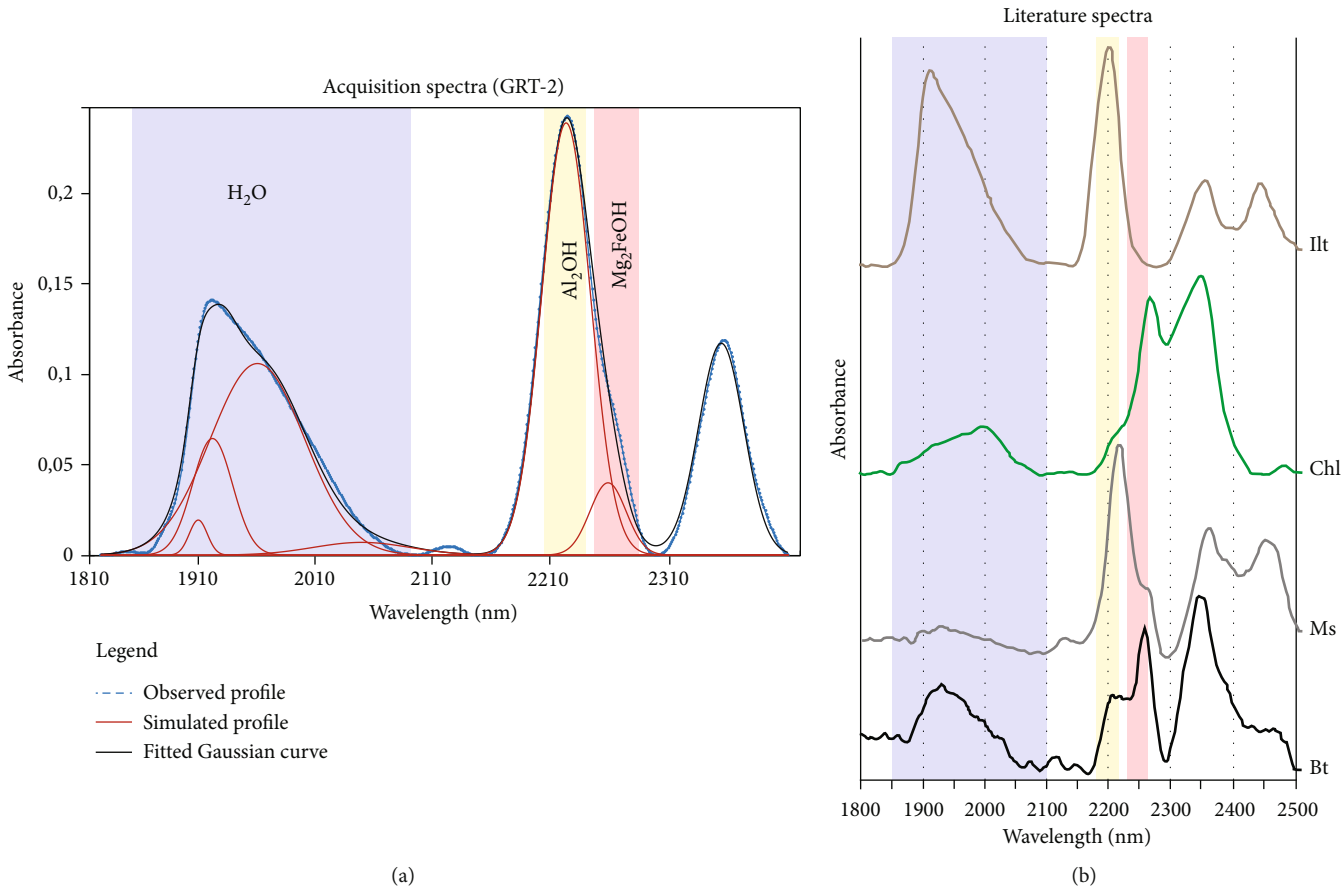

Figure 4: (a) Example of an absorption spectrum and a simulated profile in the GRT-2 well at 2800 m. (b) Reference spectra from Pontual et al. [52] for biotite (Bt), muscovite (Ms), chlorite (Chl), and illite (Ilt).

variation of 1% for the 2200 nm absorption band area, by performing five measurements without moving the sample and five measurements after mixing the sample (personal communication). Before measurements are taken, the ASD TerraSpec requires a warm-up period of approximately 30 minutes. It is also necessary to conduct a calibration with the "Spectralon" reference material provided with the machine before the first measurement and thereafter regularly every hour during the measurement period [49].

3.1.3. Processing. After the measurement, the SWIR spectra were processed with "the Spectral Swagger" (TSS), an in-house Visual Basic Macro developed at Poitiers University that runs on Microsoft Excel [49]. First, the baseline was removed automatically by the software; then, spectra were fitted with few Gaussian curves (four and two for the water and the 2200 nm absorption band areas, respectively). To create a profile simulation, the user must set the position and the half width at half maximum (HWHM). The height parameter is automatically deduced from the baseline-removed spectrum; its initial height equals 90% of the y-axis value of the baseline-removed spectrum at the Gaussian centre wavelength. The user can designate the parameter that will be allowed to change. The final simulated profile is the sum of all Gaussian curves. The quality of the fit between the simulated and observed profile is verified against the weighted profile R-factor (Rwp), which is commonly used in Rietveld refinements [50]. In this study, six Gaussian curves were used to fit the spectrum from 1820 to 2300 nm (Figure 4). For the GRT-2 well, position and HWHM were locked for each simulation profile. However, different sets of position and HWHM were used. Simulation profiles with an Rwp lower than 0.05 were accepted. For the GPK-1 well, for which a very large number of profiles (1190) were calculated, position and HWMH were free-fitted by TSS for each simulation profile. The areas of the water absorption band and the 2200 nm absorption band were also fitted manually for some profiles to determine whether there was a significant deviation in the area with respect to the free fitting. The results showed that there was no significant change in the area between profiles fitted manually and those free-fitted by TSS (see Figure S3 in the supplementary materials). Thus, the results presented in this study for the GPK-1 well are profiles that were free-fitted by TSS.

3.1.4. Mineralogical Identification. In the SWIR spectral domain, the phyllosilicates are detected, and they are not influenced by feldspars and quartz, which do not present absorption bands in this domain. Four Gaussian curves were used to fit the absorption band spanning the

wavelength range from 1900 to 2060 nm (Figure 4); this range corresponds to the stretching and bending vibrations of H_2O molecules. This absorption band exists not only for the hydrated phyllosilicates but also for some other hydrated minerals such as zeolites, opal, and amorphous silica. This absorption band can also vary according to the humidity of the environment. Hence, not only it is linked to clay minerals but also, under constant humidity conditions, the area of this absorption band will vary according to the quantity of clay minerals present in the sample. This aspect will be discussed in Section 5.2. Two Gaussian curves were used to fit the absorption band spanning the wavelength range from 2200 to 2255 nm, which mainly corresponds to the vibrations of the bonds between the cations of the octahedral sheets and the structural OH groups in the aluminous phyllosilicates, i.e., corresponding to the combination modes of the stretching and bending vibrations of the Al_2OH groups [51]. Thus, the 2200 nm absorption band represents Al-rich dioctahedral clay minerals [52]. The shoulder observed between 2247 and 2253 nm is more complex in terms of absorption band and mainly reflects the occurrence of biotite and chlorite trioctahedral clay minerals as well as of muscovite (Figure 4(a)). The Gaussian curves used to fit the spectrum from 2300 to 2400 nm are not presented in this study because we are focusing on the relative quantification of illitic minerals associated with the "Al_2OH" absorption band. In our study, the mineralogy of the granitic basement in the wells is thoroughly described by binocular magnifier observation of 240 cuttings from the GRT-2 well [33] and 1190 cuttings from the GPK-1 well [37, 53]. Thus, the variation in the relative integrated intensity of the 2200 nm absorption band is considered to represent illite variations, except in the GRT-2 well from 2950 to 3200 m MD, where significant amounts of biotite were observed, and in the GPK-1 well, in which biotite is present in the unaltered granite. Based on a comparison with spectra reported in the literature (Figure 4(b)), the influence of chlorite on the 2200 nm absorption band area is not significant, but the influence of biotite and muscovite could be significant if these minerals were present in high amounts in the studied samples. Beyond the mineralogical signature of the absorption bands, this methodology was used for a broad quantification of clay minerals based on the Beer-Lambert law, which establishes proportionality between the absorbed energy and the concentration of chemical bonds in the analysed material [54]. In this study, the area of the 2200 nm absorption band is expressed in arbitrary units (a.u.) which represents the area of the absorption band considered.

3.1.5. Intrasample Variability. Because each cuttings bag contains sections of the drilled rocks (see Section 3.1.1) and because the cuttings could not be homogeneously mixed in the bag, several measurements were performed on each cuttings bag (see Figures S1 and S2 in the supplementary materials). In the GRT-2 well, 10 measurements were performed on the same cuttings bag, whereas only 5 measurements were performed in the GPK-1 well due to the lower amount of cuttings available. Error bars were calculated for each cuttings bag to determine whether the range of variation exceeds the scattering of the data. Because the results were found to be reliable, they are not presented in this study; however, figures showing the results are provided as supplementary materials.

3.2. X-Ray Diffraction. X-ray diffraction data were acquired from selected cuttings samples of the GPK-1 well and used to identify the clay minerals present in the samples. The XRD results of Vidal et al. [18] for the GRT-2 well were also used in this study. Twenty-eight cuttings samples were collected from the GPK-1 well. The sampling was concentrated in the permeable and altered FZs as well as in the unaltered granite that was used as a reference material, as the latter is believed to be representative of rocks preserved from actual fluid circulation. The samples were not ground; they were dispersed in distilled water by ultrasonic vibration. Oriented powders on glass slides were prepared from a <5 μm clay mineral suspension obtained by sedimentation. Clay minerals were identified by XRD of air-dried and ethylene glycol-saturated oriented powders conducted on a Bruker D8 Advance diffractometer (CuKα radiation, 40 kV, 40 mA). The analytical conditions were as follows: angular domain, 2.5-30° 2θ; step increment, 0.025 2θ; and counting time per step, 1 s. XRD data acquisition and treatment were conducted using the X'Pert HighScore software (PANalytical B.V.). The clay minerals were identified according to the literature [55].

3.3. Geophysical Logs. The geophysical logs and mud logging data are presented in this study to highlight their correlations with evidence of present-day circulation (T log, He, CO_2, CH_4, and Rn), FZ evidence (neutron porosity, density, and resistivity), and evidence of the presence of paleocirculation zones rich in illite (total gamma ray, spectral potassium gamma ray (GR-K), and electrical resistivity).

3.3.1. Temperature. The T log is expressed in °C. Measurements were made every 50 cm and 10 cm in the GRT-2 and GPK-1 wells, respectively. T anomalies are interpreted as the signatures of fluid circulations between the well and the formation [30, 56–58]. For this study, the T log of the GRT-2 well was shifted upwards by 2 m from 2480 to 2650 m MD and upwards by 10 m from 2650 to 3196 m MD because stretching of the cable occurred during the measurement as a function of depth. Moreover, because the T log of the GRT-2 well was acquired separately, it could not be correlated in depth with another reference. Thus, in this study, the T log was correlated with the resistivity and porosity logs because they obviously presented the same types of anomalies preceding the four main T anomalies. For similar reasons, the T log of the GPK-1 well was shifted downwards by 7 m to vertically fit the T anomalies and the permeable FZs [30].

3.3.2. Gas Content (He, CO_2, and CH_4). The occurrence of alkanes as well as of other gas species such as He, CO_2, and CH_4 indicates permeable FZs [59, 60]. For reference, the abundances of He and CH_4 in the atmosphere are approximately 5.24 ppm and 1.75 ppm, respectively. He, CO_2, and CH_4 were monitored in GPK-1 [59]. Only CH_4 was monitored in GRT-2 [34].

3.3.3. Porosity. The neutron porosity log (NPHI) which is supposed to quantify the porosity filled with water is deduced from measurements of the hydrogen content of the formation (fast neutrons emitted by the tool are slowed down by elastic scattering, mainly due to collision with hydrogen atoms). Neutron porosity can also be highly influenced by clay minerals, which often contain bound water. It is expressed in m^3/m^3 and sometimes in %. It was sampled at every 15 cm depth in the GRT-2 and GPK-1 wells. The parameter has an investigation depth of several cm behind the borehole wall, which can correspond to the flushed zone. Porosity logs do not directly indicate true porosity in this context, a specific calibration should be performed, and the influence of the granitic matrix on the neutron porosity can be as high as 7% [61]. Nevertheless, the neutron porosity measured here provides a global signal for FZs to the extent that they are porous and contain fluids and/or clay minerals.

3.3.4. Density. The density log (RHOB) is calculated from returning gamma rays following the interaction of gamma rays emitted from a chemical source (Ce^{137} and Co^{60}) with the electrons present in the elements in the formation. These gamma rays are related to the electron density of the formation, which itself depends on the formation density. RHOB is given in g/cm and was acquired every 15 cm in depth for both the GRT-2 and the GPK-1 wells. A negative peak in a density curve could be due to the occurrence of secondary clay minerals and high porosity and thus should reveal alterations associated with a fracture zone, whereas positive peaks are associated with high-density minerals or changes in lithology.

3.3.5. Gamma Ray. The gamma ray (GR) log measures natural radioactivity (cumulative emissions, mainly from uranium (U), potassium (K), and thorium (Th)) in gAPI; vertical sampling of the GRT-2 and GPK-1 wells was performed every 15 cm. The GR log is aimed at interpreting lithology and rock composition by detecting clay minerals rich in potassium (illite and muscovite). In the altered crystalline basement, negative GR peaks in the lower positive domain can reflect drusy quartz veins in illitized host rock [14]. In the context under study, GR data are an indicator of hydrothermal alteration and thus provide information regarding paleo-permeability.

3.3.6. Electrical Resistivity. In unaltered hard rocks, the electrical resistivity log is mainly controlled by the electrical conductivity of the fluid contained in the rock porosity, a factor that is particularly significant in FZs. Electrical resistivity decreases with water saturation and is even lower for conductive fluids that contain salts, such as brines. Similarly, the electrical resistivity of clay minerals, which are conductive minerals, is low [62]. Hence, laterologs and focused resistivity arrays are sensitive to fracturation and alteration. Resistivity laterologs measure an apparent electrical resistivity that needs to be corrected for the probe characteristics, the hole effect, and spatial variations in electrical resistivity (dipping). In the zones in which hydrothermally altered granite may coexist with unaltered granite, electrical resistivity modelling should be applied to obtain the "true" electrical resistivity by taking into account the 2D/3D geometry of the zone [63]. Although petrophysical models are commonly used to evaluate hydrocarbon saturation in sedimentary formations [64]; for instance, the estimation of porosity changes from electrical resistivity is not so straightforward in fractured granitic environments. The electrical conductivity can vary by several orders of magnitudes in zones and areas with different clay mineral contents and fracture densities, whether or not the zones are sealed. In the GRT-2 well, the electrical resistivity was measured with a five-electrode configuration, yielding five apparent resistivity values (RLA1–5) [65]. The contribution of the matrix to the electrical conductivity is supposed to be far lower than that of fractures, and it can vary by several orders of magnitude among unaltered and altered granite zones [33]. Measurements were obtained every 15 cm in depth. These configurations are sensitive to the distance beyond the borehole wall. The shallowest resistivity (RLA1) mainly reflects the average resistivity of the borehole mud, and the deepest resistivity (RLA5) mainly reflects the average resistivity of the formation (granite matrix). In the GPK-1 well, the electrical resistivity was measured in 1989 using a laterolog tool with a two-electrode configuration every 15 cm in depth, yielding a shallow laterolog (LLS) and a deep laterolog (LLD). In this paper, only the most far-reaching resistivity curves (RLA5 and LLD) are presented on an inverted scale with highly resistive values on the left and conductive values on the right, allowing the reader to easily correlate GR, SWIR, and conductive peaks.

4. Results

4.1. GRT-2 Well

4.1.1. Dataset. The petrographical log of the GRT-2 well (Figure 5) was built from the macroscopic description of the alteration mineralogy in the cuttings. The hydrothermal alteration grades were determined according to the occurrence of the secondary minerals (chlorite, illite, and drusy quartz) in the cuttings samples. This petrographical log presents three major units: reddish, oxidized granite at the top of the granitic basement, an altered zone from 2535 to 3060 m MD with a highly altered core from 2737 to 2875 m MD, and unaltered granite at the bottom of the well from 3060 to 3196 m MD. These main sections correlate well with the SWIR values; more precisely, we can distinguish four sections in which the variations in the 2200 nm absorption band area are indicative of the alteration grades around the permeable FZs.

4.1.2. SWIR Variations and Hydrothermal Alteration Grades. The first section, from 2514 to 2570 m MD around the FZ1, is characterized by a small increase in the SWIR 2200 nm absorption band area, with scattered values between 6 and 10 a.u. It corresponds to the RED and HHIG facies observed with a binocular magnifier.

The second section, from 2570 to 2970 m MD, comprises the FZ2 and the FZ3 and corresponds to the HHIG and

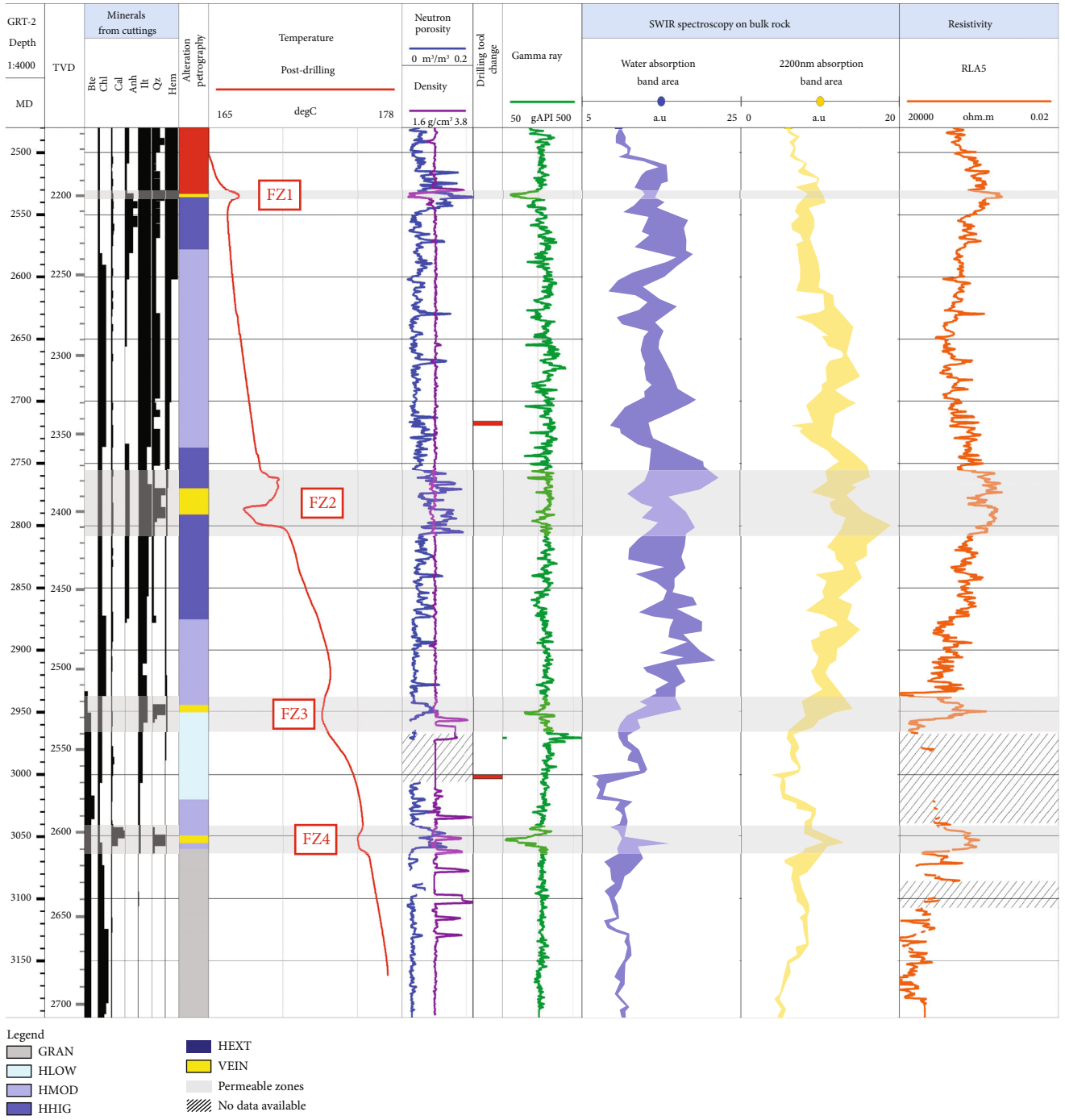

FIGURE 5: Composite log of the GRT-2 well at Rittershoffen presenting the mineral quantity, petrographical log, *T* log, porosity and density logs, drilling tool change, total GR, SWIR results with water and the 2200 nm absorption band areas, and resistivity log. Petrographical facies abbreviations are defined in the legend in Figure 3.

HMOD facies observed with a binocular magnifier. This zone is characterized by the highest values of the 2200 nm absorption band area observed for the well. These values are highly scattered between 10 and 20 a.u., and because the acoustic image logs for GRT-2 are of poor quality, it is difficult to correlate the lowest values with opened fractures. The illitization appears to increase with the alteration grade, reaching its highest value (20 a.u.) in the fracture wall (FW) at 2780 m MD. In the FZ2, minimal values of the 2200 nm absorption band area are observed for a few samples located approximately 2773 m MD. In the acoustic image logs, an opened fracture filled with secondary drusy quartz (VEIN) is observed at 2773 m MD. Below, in the deepest section, acoustic image logs are not available.

The third section, from 2970 to 3070 m MD, comprises the FZ4. The 2200 nm absorption band area appears to increase with the alteration grade, reaching its highest value (14 a.u.) in the FW at 3055 m MD, associated with a

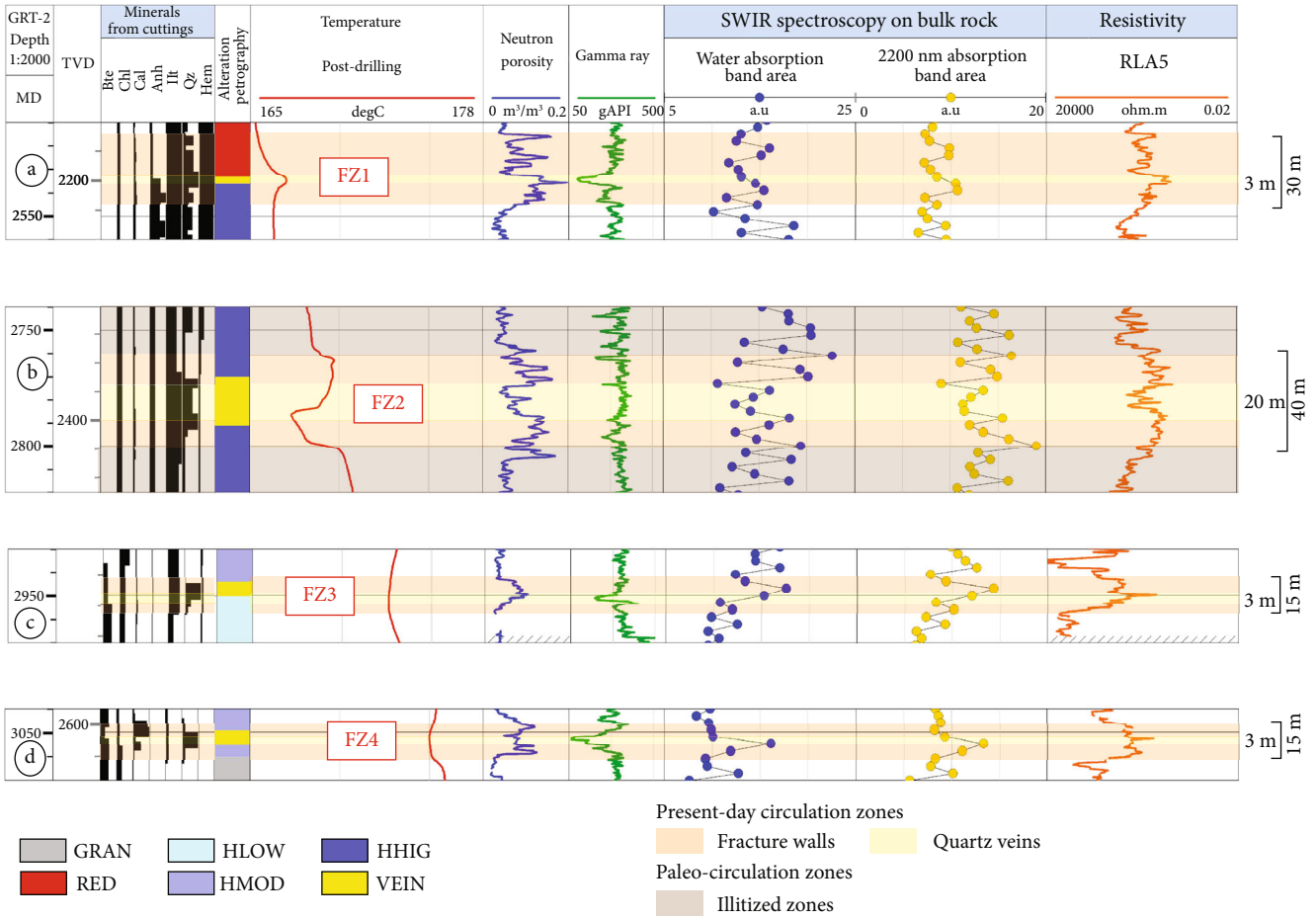

FIGURE 6: Magnified view of the four (a, b, c, and d) main permeable FZs of the GRT-2 well at Rittershoffen, presenting the mineral quantity, petrographical log, *T* log, porosity and density logs, total GR, SWIR results with water and the 2200 nm absorption band areas, and resistivity log (low values to the right). Petrographical facies abbreviations are defined in the legend in Figure 3.

permeable FZ and a quartz vein at 3050 m MD. This zone corresponds to the HMOD and HLOW facies observed with a binocular magnifier.

The fourth section, from 3070 to 3196 m MD, corresponds to the GRAN facies observed with a binocular magnifier. The values of the 2200 nm absorption band area are stable and low, ranging from 5 to 8 a.u.

The resistivity log also appears to correlate relatively well with the trend of the SWIR log (2200 nm absorption band area). In the open hole of the GRT-2 well, 500 m is altered granite and 200 m is unaltered granite. Thus, altered granite represents 70% of the open-hole section.

4.1.3. Permeable FZs. The four permeable FZs of the GRT-2 well are shown in Figure 6 and are discussed below.

(1) FZ1 (2533 m MD). From the ultrasonic borehole images (UBI), no small-scale fracture is observed around the quartz vein for this FZ [34]. The porosity log shows high, scattered values in the entire FZ, the GR log exhibits a low peak correlated with the quartz vein, and the resistivity log shows a high conductivity peak that is also correlated with the quartz vein (Figure 6(a)). The thermal anomaly is localized at the quartz vein depth. The SWIR absorption band area at 2200 nm shows scattered and average values. According to the geophysical logs, the natural flow appears to be spatially correlated with the occurrence of a quartz vein. The observed conductivity peak in this permeable quartz vein could be due to the presence of geothermal brine, which is a very conductive fluid [66].

(2) FZ2 (2770 m MD). The UBI is not available over the entire zone, but open fractures are observed at 2767, 2770, and 2774 m MD and are associated with the occurrence of quartz veins, translating into potential open pathways for fluids. Below these open fractures, smaller sealed fractures are observed from 2786 to 2789 m MD [34]. Whereas the GR is quite stable with some small negative peaks, the porosity, electrical conductivity, and SWIR 2200 nm absorption band area present two positive humps extending vertically over a length of 40 m (Figure 6(b)). This zone is the most contributive according to hydraulic tests [31], but the intra-FZ section reveals a complex architecture. At the centre of the zone, resistive values are observed (from 2776 to 2783 m MD), correlating with low neutron porosity, whereas the GR is unaffected, which goes along with the presence of the quartz vein observed in the cuttings. More generally, the observations in this FZ are consistent with a permeable FZ and brine

circulations. The lack of UBI data in this zone does not help support our interpretation. However, the fact that the unavailability of UBI data is due to difficulties in running the tool in this zone because of cavings also suggests the existence of an FZ.

(3) FZ3 and FZ4 (2950 and 3052 m MD). No UBI is available for this zone; thus, we are unable to describe the architecture of the FZs. The presence of *T* anomalies implies circulation in both FZs. These two FZs look alike. In fact, they present a neutron porosity increase over 10 m, a low GR, and a sharp peak in electrical conductivity correlated with the quartz veins (Figures 6(b) and 6(c)). Two higher resistivity values are observed above and below the FW, surrounding the zone of higher neutron porosity. These peaks appear to be related to the presence of unaltered (or slightly altered) granite, which occurs from 2934 m MD according to the high resistive values and also appears to be correlated with the SWIR values, which are stable and low at this depth. The SWIR 2200 nm absorption band area is high in both of these FZs. For both FZs, the sharp increase in electrical conductivity appears to be linked to brine circulation in the quartz veins, whereas the lower conductive values above and below the quartz veins appear to be linked to the occurrence of illite in the FW. The abrupt decrease in electrical conductivity suggests a closely delimited hydrothermal circulation zone.

4.2. GPK-1 Well

4.2.1. Dataset. The petrographical log of the GPK-1 well was compiled by Genter et al. [42, 43] and Traineau et al. [37] from cuttings samples based on macroscopic observations with a binocular magnifier. The grades of hydrothermal alteration were determined according to the occurrence of the secondary minerals (chlorite, illite, and drusy quartz) in the cuttings samples. This petrographical log presents three major hydrothermally altered granite units surrounded by unaltered granite. These three units extend from 1580 to 1830 m MD, from 2600 to 2800 m MD, and from 3200 to 3500 m MD.

4.2.2. SWIR Variations and Hydrothermal Alteration Grades. The first section, from 1580 to 1830 m MD, is characterized by very scattered high values between 3 and 26 a.u. for the 2200 nm absorption band area. The shift of the SWIR values to high values in this section could be due to a granulometry effect, as this section was drilled first and was then deepened, resulting in a change in the cuttings grain size. Based on binocular magnifier observations, this section corresponds to GRAN with hydrothermally altered zones of HMOD-HHIG facies. These altered zones appear to correlate with the SWIR values, which are higher, i.e., between 8-17 a.u. for the 2200 nm absorption band area for HMOD (1547-1553 m MD, 1579-1606 m MD, and 1650-1656 m MD) and approximately 25 a.u. for HHIG (at 1620-1640 m MD). Quartz veins were identified at 1645 m MD (FZ1) and at 1814 m MD (FZ2), where drusy quartz was visible by observations of cuttings. The latter corresponds to a fracture vein that is visible in core samples (Figure 7).

The second section, from 2605 to 2827 m MD, is characterized by high, scattered values between 3 and 19 a.u. for the 2200 nm absorption band area. Based on binocular magnifier observations, it corresponds to GRAN with occurrences of low to high hydrothermal alterations. The HLOW grade appears to correlate with the 2200 nm absorption band area, with values between 5 and 10 a.u. at 2600-2603 m MD, 2610-2612 m MD, 2676-2679 m MD, 2681 m MD, 2693-2701 m MD, and 2731-2733 m MD. Occurrences of HMOD suggest a good correlation with the 2200 nm absorption band area, with values between 7 and 15 a.u. at 2625-2632 m MD, 2679-2681 m MD, 2685-2692 m MD, 2701-2731 m MD, and 2733-2736 m MD. The HHIG occurrences also suggest a good correlation with the stable values of the 2200 nm absorption band area, which range from 14 to 19 a.u. A quartz vein is observed in the cuttings from 2817 to 2818 m MD (FZ3). An open fracture is observed on the FMI log and is characterized by the occurrence of He and CO_2 content, evidencing the presence of geothermal fluid.

The third section, from 3203 to 3523 m MD, is characterized by high, scattered values between 3 and 19 a.u. for the 2200 nm absorption band area. Based on binocular magnifier observations, it corresponds to GRAN with occurrences of hydrothermal alterations of HLOW to HEXT facies. HLOW appears to correlate with values of the 2200 nm absorption band area between 4 and 8 a.u. Two quartz veins are observed in the same fracture zone at 3489 and 3496 m MD in the cuttings. These open fractures, which match the flow log anomalies, are observed on the acoustic image logs at 3490 and at 3495 m MD (FZ4).

Outside of these sections, from 2065 to 2605 m MD and from 2827 to 3203 m MD, we observe low, very stable values between 2 and 9 a.u. for the 2200 nm absorption band area. Based on binocular magnifier observations, these correspond to GRAN, with HLOW-HMOD from 2505 to 2530 m MD. These hydrothermal alteration grades suggest a good correlation with the 2200 nm absorption band area which presents higher values of approximately 9 a.u.

In the open-hole section of the GPK-1 well, 500 m is hydrothermally altered granite and 2200 m is unaltered granite; thus, the hydrothermally altered granite represents only 20% of the open hole.

4.2.3. Permeable FZs. The two FZs of the upper section of the GPK-1 well (1540-2000 m MD) are shown in Figure 8 and are discussed below.

(1) FZ1 (1645 m MD). A quartz vein was observed, and a *T* anomaly above the quartz vein proves a contributive flow zone (Figure 8(a)). The porosity presents high values above and below the quartz vein, whereas low values are observed at the quartz vein depth. The GR-K is also slightly higher above and below the quartz vein, whereas it is low at the quartz vein. Very small He content is also visible above the quartz vein. The laterolog resistivity (LLD) presents high conductivity values above the quartz vein and high resistivity values at the quartz vein depth. He content is also observed in this section, indicating the occurrence of dissolved gas in the geothermal fluid (Figures 7 and 8). The SWIR values are high

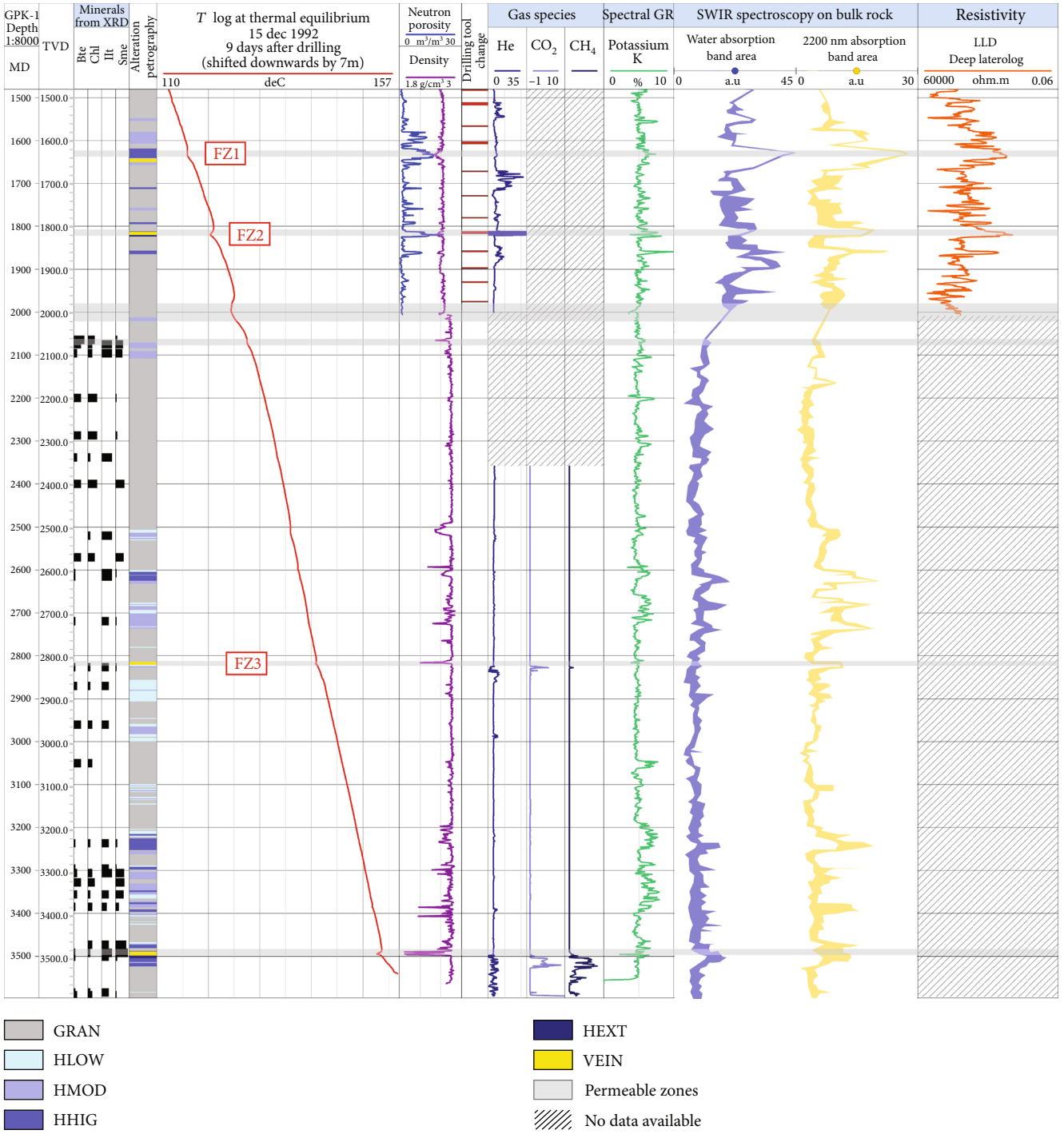

Figure 7: Composite log of the GPK-1 well at Soultz-sous-Forêts, presenting the mineral quantity, petrographical log, *T* log, porosity and density logs, drilling tool change, gas species, spectral GR-K, SWIR results with water and 2200 nm absorption band areas, and resistivity log. Petrographical facies abbreviations are defined in the legend in Figure 3.

in the FZ, particularly above the quartz vein. The hydraulic data show that flow anomalies are mainly due to the FZ core [67]. However, surprisingly, the quartz vein presents neither a sharp *T* anomaly nor evidence of fluid circulations from geophysical logs. The geophysical anomalies associated with the FW above the sealed quartz vein could suggest that the FW corresponds to porous granite which allows a good connection between the well and the near-well field. On the other hand, the geophysical anomalies of the FW below the quartz vein could indicate that the FW acts as a tight zone possibly caused by secondary mineral precipitations.

(2) FZ2 (1814 m MD). This FZ presents a localized *T* anomaly correlated with the quartz vein (Figure 8(b)). According to this *T* anomaly and considering the section between 1400 and 2000 m, the majority of the fluid flows from this FZ

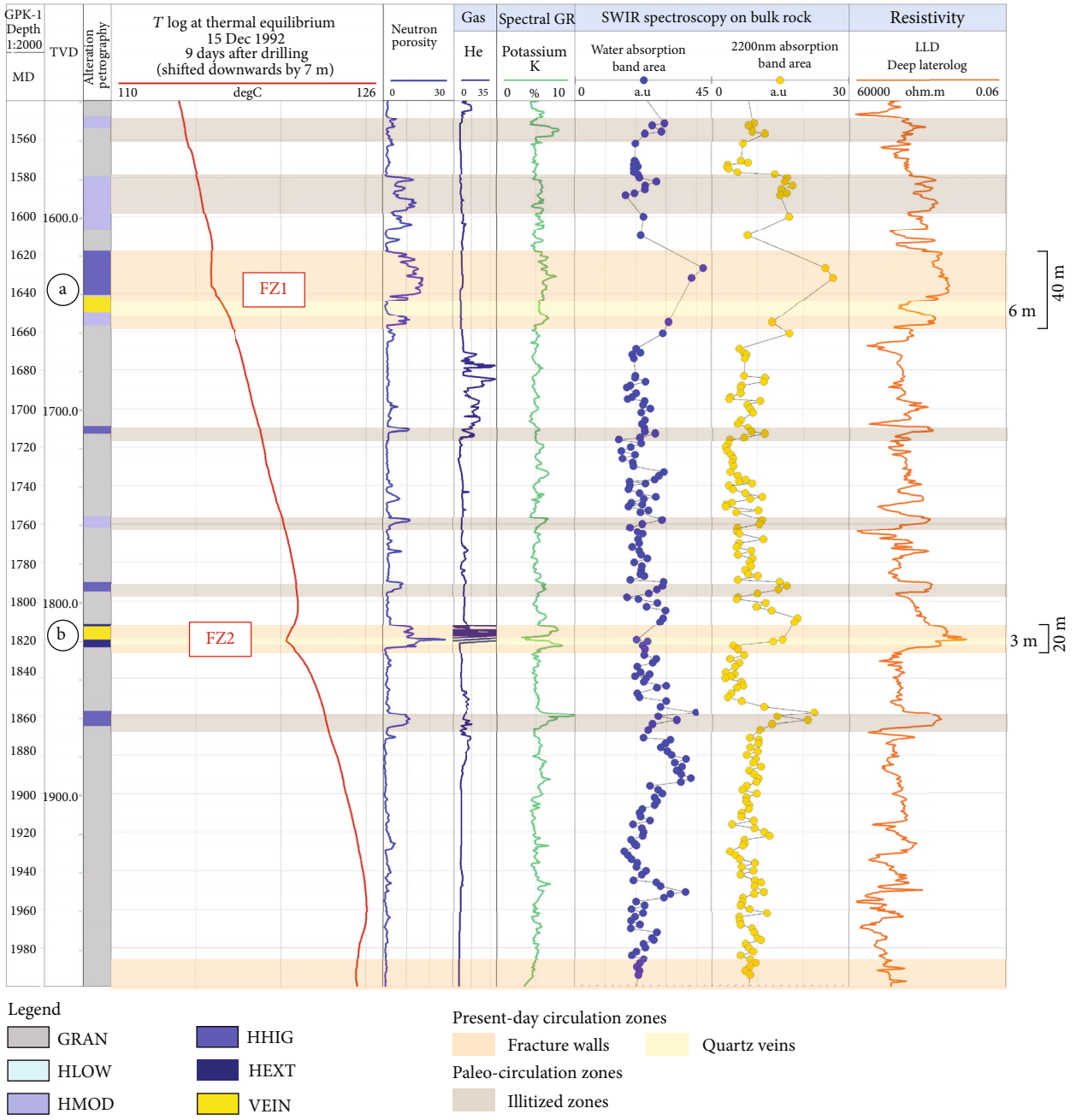

FIGURE 8: Magnified view of two (a and b) main permeable FZs of the GPK-1 well at Soultz-sous-Forêts, presenting the petrographical log, *T* log, porosity and density logs, spectral GR-K, SWIR results with water and 2200 nm absorption band areas, and resistivity log. Petrographical facies abbreviations are defined in the legend in Figure 3.

[67, 68]. The porosity is high and shows a sharp peak in its centre that is correlated with the drusy quartz vein. The GR-K presents a low peak at the quartz vein depth and high peaks in the FW above and below the quartz vein. The resistivity laterolog presents high electrical conductivity values, with a sharp very conductive peak at the quartz vein depth, and lower-than-average resistivity values above and below that are correlated with the FWs. The SWIR 2200 nm absorption band area presents higher values in the FZ. As for FZ3 and FZ4 in the GRT-2 well, the sharp and very high conductivity values could be associated with the brine circulating in the quartz vein since high GR-K and the conductive zone above and below coincide with the high amount of clay minerals (illite) in the FW. The very high He content matching the quartz vein (>200 ppm) evidences the occurrence of permeability indicators such as geothermal gases dissolved in the brine.

5. Discussion

5.1. SWIR as a Permeability Indicator. The SWIR method showed good reproducibility of the measurements obtained

on cuttings samples. Stable and low values appear to be systematically observed in conjunction with the unaltered or slightly hydrothermally altered granite (Figures 5, 7, and 9). The geothermal reservoirs of the Soultz and Rittershoffen geothermal sites are highly fractured, with fracture infillings corresponding to secondary drusy quartz and some carbonates, and present hydrothermally altered zones. The heterogeneity of the hydrothermal facies encountered produces heterogeneity in the SWIR signal that appears on the SWIR log as peaks exceeding the mean values, surely reflecting the presence of mineralizations associated with hydrothermal circulations. Because the primary and secondary mineralogy of the deep granites in the URG basement does not vary significantly, the SWIR method is easily applicable to the detection of fluid-rock interaction processes linked to geothermal fluid circulation in the granitic fractured reservoirs of geothermal wells. More generally, the combination of the SWIR 2200 nm absorption band area and the spectral GR-K is a strong illite indicator. On a large scale, the scattering (linked to quartz vein occurrences in the FZs) and the high values of the SWIR 2200 nm absorption band area localize the highly altered zones crossed by the wells. These highly altered zones are linked to the main faults and are interpreted as the permeable zones of the well (Figures 6 and 8). The vertical extent of this scattering provides in-depth information on the extent of the well volume that is affected by hydrothermal circulations. This initial study applying the SWIR method to the Soultz and Rittershoffen geothermal sites will soon be reinforced by an ongoing study in which the SWIR method is applied to the new Illkirch geothermal site. This will help us confirm our interpretation and extend the interpretation to the URG.

Based only on geophysical logs (acoustic image logs were not acquired below 2850 m MD), the main permeable FZ of GRT-2 was identified from 2766-2800 m MD with a true thickness of 35 m by Vidal et al. [34]. Our SWIR method yields new complementary results that provide new information about the FZ architecture, and we observe that the FZ is more extended than was described by Vidal et al. [34] based on geophysical logs. SWIR helps distinguish the part of the actual FZ that controls the present-day circulations and the part of the FZ that has been affected by paleo-circulations. In fact, this study using SWIR data reveals that this zone presents an intense illitization extending from 2743 to 2884 m MD and thus a true thickness of 112 m. Previous mineralogical studies of the GRT-2 well suggested that a low intensity of illitization could explain the high permeability of the well [18]. However, the GRT-2 well presents high values of the 2200 nm absorption band area (20 a.u.); these are higher than the values measured in the GPK-1 well (13 a.u.) and also higher than those measured in other wells such as GRT-1 and GPK-4 [69]. These high SWIR 2200 nm absorption band area values are surprising considering the results of Vidal et al. [18]. The advantage of the SWIR method is that it provides a general and continuous overview of the well in terms of permeability indicators that prevents over-interpretation of punctual localized data.

5.2. SWIR Correlation. From simple observations, for both the GRT-2 and GPK-1 wells, the water absorption band area and the 2200 nm absorption band area appear to be correlated (Figures 5 and 7). In fact, the ratio between the water absorption band area and the 2200 nm absorption band area varies significantly according to the species of aluminous phyllosilicates considered (illite and micas) [21].

The correlation between these two absorption bands was tested for both wells (Figure 9). For the GRT-2 well, the correlation appears to be linear with a correlation coefficient of 0.62 (Figure 9(a)). For the GPK-1 well, the correlation presents two linear tendencies (Figure 9(a)). After classifying the samples into altered and unaltered granite on the basis of petrographic observations, it was found that these two tendencies correspond to hydrothermally altered granite with a coefficient of 0.53 and to unaltered granite with a coefficient of 0.26 (Figure 9(a)).

From mineralogical identifications (XRD and binocular magnifier observations), the unaltered granite in both wells is characterized by the presence of biotite and chlorite whereas the altered granite is essentially characterized by the presence of illite and illite-rich illite/smectite mixed layers in considerable amounts (Figures 9(b) and 9(c)).

Based on the phyllosilicate mineralogy of the unaltered and altered granite, it seems relevant to use the 2200 nm absorption band area as an indicator of the illitization rate of the granitic rocks of Northern Alsace. In the GPK-1 well, we can clearly see that for a similar value of the water absorption band area (e.g., a water absorption band area of 20 a.u.), we observe values of the 2200 nm absorption band area of the illitized granite more than two times higher than those observed for the unaltered granite (17 a.u. and 7 a.u., respectively). Considering the absorption band area at 2200 nm, the lower absorption depth noted for the samples of unaltered granite (Figure 9) can be explained by a weak to very weak contribution of both primary biotite and chlorite to the absorption band near 2200 nm (Figure 4(b)). The correlation between the water absorption band area and the 2200 nm absorption band area indicates that the mineralogy of the GRT-2 well is more homogeneous than that of the GPK-1 well (Figure 9).

From the SWIR results, the GRT-2 well showed a higher degree of hydrothermal alteration all along the well compared to the GPK-1 well. In this well, unaltered granite presents some localized sharp peaks of the 2200 nm absorption band area that correspond to the fracture-controlled altered zones. The interpretation of the two correlation tendencies of the GPK-1 well is consistent along with the petrographical observations: localized FZs are intersected on small apparent depth extents (Figures 7 and 9). These mineralogical and structural differences between the wells are explained by their different trajectories and concepts. Notably, the GPK-1 well was drilled nearly vertically and intersects few localized FZs at a higher angle, whereas the GRT-2 well is highly deviated but has an orientation parallel to the Rittershoffen local fault over its approximately 400 m apparent length. In fact, the GPK-1 well required stimulation, whereas the GRT-2 well did not, suggesting that intense illitization is a good indicator of permeability.

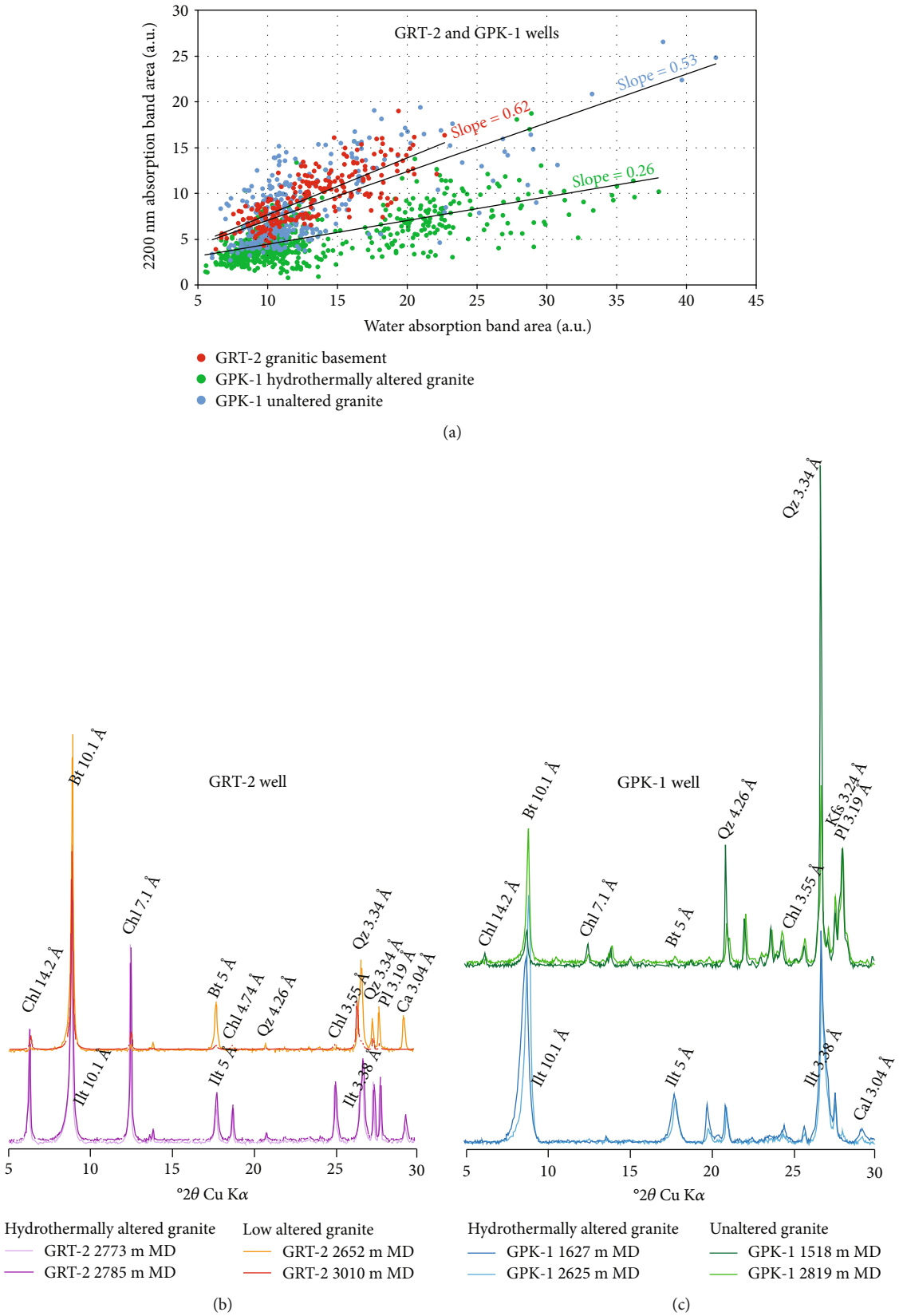

Figure 9: Correlation of the SWIR water and 2200 nm absorption band area for (a) the GRT-2 and GPK-1 wells, (b) XRD results for the slightly altered granite and the hydrothermally altered granite in the GRT-2 well, and (c) XRD results for the unaltered granite and the hydrothermally altered granite in the GPK-1 well.

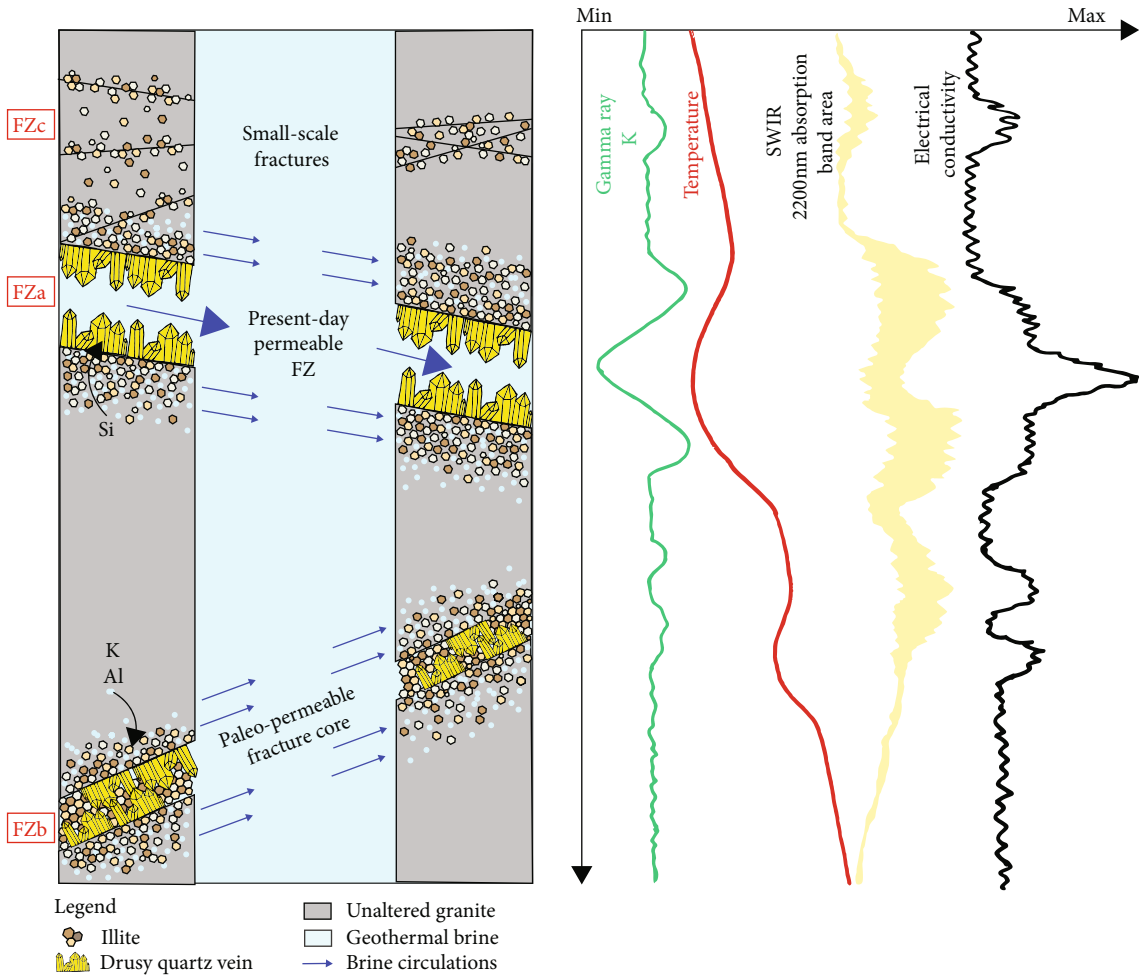

Figure 10: Model showing the variation in the 2200 nm absorption band area and its correlation with geophysical logs (gamma ray, temperature, and electrical conductivity) in response to different grades of hydrothermal alteration of the granite and different FZ architectures.

5.3. Electrical Logs and SWIR. The similar shapes and tendencies observed for the electrical logs and the SWIR data, outside of brine circulation in FZs, at first show a considerable control of illite on the electrical properties measured in the GRT-2 and GPK-1 wells (Figure 10). Very conductive zones are often associated with the SWIR 2200 nm absorption band area and with high GR-K peaks pointing to highly hydrothermally altered zones rich in illite. This type of zone could be observed either associated with a *T* anomaly, yielding an altered zone that is contributive (in FZ1 at 1620-1640 m MD in GPK-1) (Figure 8(a)), or with a straight *T* profile, yielding a sealed illitized zone (at 1550, 1579-1606, 1710, 1758, 1792, and 1860 m MD in GPK-1), which could be paleo-circulation zones (Figure 8). Resistive peaks can correlate with negative 2200 nm absorption band area peaks and the occurrence of a quartz vein, suggesting a fracture core plugged with secondary drusy quartz filling with insufficient residual porosity for abundant circulation and no abundant illite (low GR) (FZ1 at 1645 m MD in GPK-1) (Figure 8(a)). At a more restricted level, positive conductivity peaks can also correlate with negative GR-K peaks, low SWIR 2200 nm absorption band area, and *T* anomalies, translating into the presence of brine such as in the cores of FZs (FZ2 at 1814 m in GPK-1, FZ1 at 2534 m MD, FZ3 at 2950 m MD, and FZ4 at 3050 m MD in GRT-2) (Figures 6 and 8).

5.4. FZ Signatures. In the GRT-2 well, FZs are always correlated with *T* anomalies and VEIN facies. This observation is probably related to the drusy euhedral quartz geometry, which keeps the space open and prevents plugging of the fracture. In contrast, the textural organization of illite in the FWs tends to plug the zone (Figure 10).

A specific signature of the resistivity laterolog is observed in both the GRT-2 and GPK-1 wells (FZ3 and FZ4 in GRT-2 and FZ2 in GPK-1), with very low resistivity values (20 ohm·m) corresponding to the occurrence of geothermal brine within the quartz vein as well as low resistivity values (20 ohm·m) corresponding to illite occurrence in the FW (Figures 6, 8, and 10).

We can distinguish three types of FZs (Figure 10):

(i) FZa: permeable FZs with localized brine contributions, such as FZ1, FZ3, and FZ4 in GRT-2

(Figures 6(a), 6(c), and 6(d)) and FZ2 in GPK-1 (Figures 6(a), 6(c), 6(d), 8(b), and 10)

(ii) FZb: permeable FZs with multiple brine contributions, such as FZ2 in GRT-2 and FZ1 in GPK-1 (Figures 6(b), 8(a), and 10)

(iii) FZc: paleo-permeable FZs, such as those at 1550, 1579-1606, 1710, 1758, 1792, and 1860 m MD in GPK-1 (Figures 8 and 10)

Evans et al. [70] showed that in the open-hole section of GPK-1, the poststimulated flow zones systematically match the permeable and paleo-permeable FZs.

5.5. Applications. In future geothermal projects in the URG, the SWIR method could be a routine mud logging method. As a matter of fact, along with GR measurements obtained while drilling (MWD), cuttings provide the first data obtained during drilling. The use of SWIR measurements during drilling, when previously calibrated with the granitic analogue signature, could be helpful in determining the extent of the hydrothermally altered fault damage zone and in quantifying the alteration grade encountered in the granite. This could help determine when the exploration well leaves the altered zone and thus when to stop drilling. The SWIR method could be used as a routine mud logging analysis on-site during drilling after washing and drying the cuttings samples. It could also be further refined for the alteration mineralogy identification in geothermal systems [21].

In enhanced geothermal system projects, SWIR could be used to target paleo-permeable zones that could be reopened (sealed fractures and damage zones), thereby enhancing the permeability between the well and the reservoir during stimulation operations. In a similar manner, for existing geothermal wells in the URG drilled in granite, SWIR could be used as a complementary method to precisely characterize the hydrothermal alterations around the FZs and to target potential stimulation zones in cases of decreased productivity.

6. Conclusion

In this paper, the analysis of the correlation between the SWIR water and 2200 nm absorption bands areas confirms the petrography observed in both wells. By showing that the mineralogy is more homogeneous in the GRT-2 well than in the GPK-1 well, the results confirm that the two wells do not crosscut the circulation zones in the same way. Showing that the fluid-rock ratio is higher in the GRT-2 well than in the GPK-1 well, these results are consistent, according to hydrothermal concepts, with the higher productivity of the GRT-2 well compared to the GPK-1 well, which required stimulation. In this study, we observe three types of FZs: FZs with a localized contribution, FZs with multiple contributions, and paleo-permeable FZs. In conclusion, the SWIR method is a robust method for the detection of paleo- and present circulation zones for geothermal applications. By the joint interpretation of SWIR data and other geophysical logs, this method could be used to determine whether the studied zone is a currently active circulation zone or a paleo-circulation zone. According to the values of the SWIR 2200 nm absorption band area, grades of alteration as well as the fluid-rock ratio trend can be determined. The similar variations in the SWIR 2200 nm absorption band area and the electrical logs demonstrate a significant influence of the rock clay mineral content (quantity of illitic minerals) on the electrical response. A specific electrical signature is observed in each well, indicating the FZ architecture and brine or illite contributions.

Data Availability

Data of the Rittershoffen wells belong to ECOGI. Please contact ES-Géothermie for data requests at geothermie@es.fr. Data of the Soultz wells can be requested at guichet.H@brgm.fr. SWIR data belong to ES-Géothermie and Poitiers University; for data request, please contact geothermie@es.fr.

Conflicts of Interest

The authors declare that they have no competing interests.

Authors' Contributions

CG acquired the SWIR data in GPK-1. JV acquired the SWIR data in GRT-2. CG, JV, PP, DB, SP, and AG worked on the interpretation of SWIR data and the correlation with other geophysical logs. CG and J-FG worked on the interpretation of the electrical logs. All authors approved the final manuscript.

Acknowledgments

This manuscript was prepared as a contribution to the PhD thesis (University of Strasbourg) of Carole Glaas which is cofunded by ES-Géothermie and ANRT (French Agency for Research and Technology). The authors warmly thank Benoît Hébert for allowing them to use his in-house Visual Basic software (TSS) and the Poitiers University team for the use of the TerraSpec on the Soultz site. They warmly thank Chrystel Dezayes from BRGM for the access to the Soultz cuttings samples. The authors acknowledge the EGS Alsace and DEEP-EM projects funded by ADEME (French Agency for Environment), GEIE EMC, and ECOGI for providing the Soultz and Rittershoffen cuttings samples and logs. Sophie Funfrock is thanked for improving the manuscript with English revision. Tom Schintgen is also thanked for the review of the manuscript.

Supplementary Materials

This supporting information provides details on the SWIR results acquired in the GRT-2 and GPK-1 wells. Figure S1 shows the intrasample variability in the GPK-1 well, presenting the results of multiple measurements of the same cuttings samples. Figure S2 shows the intrasample variability in the GRT-2 well, presenting the results of multiple measurements

of the same cuttings samples. Figure S3 presents a comparison between manual fitting of the data for the GPK-1 well and automatic fitting of the same data using the TSS software. *(Supplementary Materials)*

References

[1] M. E. Schumacher, "Upper Rhine Graben: role of preexisting structures during rift evolution," *Tectonics*, vol. 21, no. 1, pp. 6-1–6-17, 2002.

[2] T. Villemin and F. Bergerat, "L'évolution structurale du fossé rhénan au cours du Cénozoïque : un bilan de la déformation et des effets thermiques de l'extension," *Bulletin de la Société Géologique de France*, vol. 8, pp. 245–255, 1987.

[3] P. Baillieux, E. Schill, J.-B. Edel, and G. Mauri, "Localization of temperature anomalies in the Upper Rhine Graben: insights from geophysics and neotectonic activity," *International Geology Review*, vol. 55, no. 14, pp. 1744–1762, 2013.

[4] C. Dezayes and C. Lerouge, "Reconstructing paleofluid circulation at the Hercynian basement/Mesozoic sedimentary cover interface in the Upper Rhine Graben," *Geofluids*, vol. 2019, Article ID 4849860, 30 pages, 2019.

[5] R. Schellschmidt and C. Clauser, "The thermal regime of the Upper Rhine Graben and the anomaly at Soultz," *Zeitschrift für Angewandte Geologie*, vol. 42, pp. 40–44, 1996.

[6] C. Dezayes, A. Genter, and B. Valley, "Structure du reseau de fractures naturelles dans le reservoir geothermique peu permeable de Soultz," *Comptes Rendus Geoscience*, vol. 342, no. 7-8, pp. 517–530, 2010.

[7] J. Sausse and A. Genter, "Types of permeable fractures in granite," *Geological Society, London, Special Publications*, vol. 240, no. 1, pp. 1–14, 2005.

[8] V. F. Bense, T. Gleeson, S. E. Loveless, O. Bour, and J. Scibek, "Fault zone hydrogeology," *Earth-Science Reviews*, vol. 127, pp. 171–192, 2013.

[9] S. S. Berg and E. Øian, "Hierarchical approach for simulating fluid flow in normal fault zones," *Petroleum Geoscience*, vol. 13, no. 1, pp. 25–35, 2007.

[10] J.-H. Choi, P. Edwards, K. Ko, and Y.-S. Kim, "Definition and classification of fault damage zones: a review and a new methodological approach," *Earth-Science Reviews*, vol. 152, pp. 70–87, 2016.

[11] D. R. Faulkner, C. A. L. Jackson, R. J. Lunn et al., "A review of recent developments concerning the structure, mechanics and fluid flow properties of fault zones," *Journal of Structural Geology*, vol. 32, no. 11, pp. 1557–1575, 2010.

[12] C. E. Manning and S. E. Ingebritsen, "Permeability of the continental crust: implications of geothermal data and metamorphic systems," *Reviews of Geophysics*, vol. 37, no. 1, pp. 127–150, 1999.

[13] J. Vidal and A. Genter, "Overview of naturally permeable fractured reservoirs in the central and southern Upper Rhine Graben: insights from geothermal wells," *Geothermics*, vol. 74, pp. 57–73, 2018.

[14] A. Genter, H. Traineau, B. Ledésert, B. Bourgine, and S. Gentier, "Over 10 Years of Geological Investigations within the HDR Soultz Project, France," in *Presented at the World Geothermal Congress*, pp. 3707–3712, Kyushu, Japan, 2000.

[15] G. R. Hooijkaas, A. Genter, and C. Dezayes, "Deep-seated geology of the granite intrusions at the Soultz EGS site based on data from 5 km-deep boreholes," *Geothermics*, vol. 35, no. 5-6, pp. 484–506, 2006.

[16] B. Ledésert, G. Berger, A. Meunier, A. Genter, and A. Bouchet, "Diagenetic-type reactions related to hydrothermal alteration in the Soultz-sous-Forêts granite, France," *European Journal of Mineralogy*, vol. 11, no. 4, pp. 731–742, 1999.

[17] C. Meller and T. Kohl, "The significance of hydrothermal alteration zones for the mechanical behavior of a geothermal reservoir," *Geothermal Energy*, vol. 2, no. 1, pp. 1–21, 2014.

[18] J. Vidal, P. Patrier, A. Genter et al., "Clay minerals related to the circulation of geothermal fluids in boreholes at Rittershoffen (Alsace, France)," *Journal of Volcanology and Geothermal Research*, vol. 349, pp. 192–204, 2018.

[19] B. Ledésert, R. Hebert, A. Genter, D. Bartier, N. Clauer, and C. Grall, "Fractures, alterations hydrothermales et permeabilite dans l'echangeur geothermique de Soultz," *Comptes Rendus Geoscience*, vol. 342, no. 7-8, pp. 607–615, 2010.

[20] Y. Rotstein, J.-B. Edel, G. Gabriel, D. Boulanger, M. Schaming, and M. Munschy, "Insight into the structure of the Upper Rhine Graben and its basement from a new compilation of Bouguer gravity," *Tectonophysics*, vol. 425, no. 1-4, pp. 55–70, 2006.

[21] M. P. Simpson and A. J. Rae, "Short-wave infrared (SWIR) reflectance spectrometric characterisation of clays from geothermal systems of the Taupō Volcanic Zone, New Zealand," *Geothermics*, vol. 73, pp. 74–90, 2018.

[22] J. D. Garnish, *Hot dry rock - a European perspective*, GRC Hawaï, 1985.

[23] A. Gérard and O. Kappelmeyer, "The Soultz-sous-Forets project," *Geothermics*, vol. 16, no. 4, pp. 393–399, 1987.

[24] A. Gérard, A. Menjoz, and P. Schwoerer, "L'anomalie thermique de Soultz-sous-Forêts," *Géothermie Actualités*, vol. 3, pp. 35–42, 1984.

[25] O. Kappelmeyer, "European HDR project at Soultz-sous-Forêts general presentation," *Geothermal Science and Technology*, vol. 4, pp. 263–289, 1991.

[26] R. Jung, "Connecting a borehole to a nearby fault by means of hydraulic fracturing," in *Geothermal Resources Council Transactions*, vol. 16, pp. 433–437, 1992.

[27] E. Schill, A. Genter, N. Cuenot, and T. Kohl, "Hydraulic performance history at the Soultz EGS reservoirs from stimulation and long-term circulation tests," *Geothermics*, vol. 70, pp. 110–124, 2017.

[28] A. Genter, K. Evans, N. Cuenot, D. Fritsch, and B. Sanjuan, "Contribution of the exploration of deep crystalline fractured reservoir of Soultz to the knowledge of enhanced geothermal systems (EGS)," *Comptes Rendus Geoscience*, vol. 342, no. 7-8, pp. 502–516, 2010.

[29] T. GeOrg, "EU-Projekt GeORG - Geoportal [WWW Document]," 2017, http://www.geopotenziale.org/home?lang=3.

[30] J. Vidal, R. Hehn, C. Glaas, and A. Genter, "How can temperature logs help identify permeable fractures and define a conceptual model of fluid circulation? An example from deep geothermal wells in the Upper Rhine Graben," *Geofluids*, vol. 2019, Article ID 3978364, 14 pages, 2019.

[31] C. Baujard, A. Genter, E. Dalmais et al., "Hydrothermal characterization of wells GRT-1 and GRT-2 in Rittershoffen, France: implications on the understanding of natural flow systems in the Rhine Graben," *Geothermics*, vol. 65, pp. 255–268, 2017.

[32] C. Baujard, A. Genter, N. Cuenot et al., "Experience from a Successful Soft Stimulation and Operational Feedback after 2

Years of Geothermal Power and Heat Production in Rittershoffen and Soultz-sous-Forêts Plants (Alsace, France)," in *Presented at the Geothermal Resource Council*, pp. 2241–2252, Reno, Nevada, USA, 2018.

[33] C. Glaas, A. Genter, J. F. Girard, P. Patrier, and J. Vidal, "How do the geological and geophysical signatures of permeable fractures in granitic basement evolve after long periods of natural circulation? Insights from the Rittershoffen geothermal wells (France)," *Geothermal Energy*, vol. 6, no. 1, pp. 1–25, 2018.

[34] J. Vidal, A. Genter, and F. Chopin, "Permeable fracture zones in the hard rocks of the geothermal reservoir at Rittershoffen, France," *Journal of Geophysical Research: Solid Earth*, vol. 122, no. 7, pp. 4864–4887, 2017.

[35] A. Genter and H. Traineau, "Analysis of macroscopic fractures in granite in the HDR geothermal well EPS-1, Soultz-sous-Foreˆts, France," *Journal of Volcanology and Geothermal Research*, vol. 72, no. 1-2, pp. 121–141, 1996.

[36] A. Cocherie, C. Guerrot, C. M. Fanning, and A. Genter, "U-Pb dating of two granite types from Soultz (Rhine Graben, France)," *Comptes Rendus Geoscience*, vol. 336, no. 9, pp. 775–787, 2004.

[37] H. Traineau, A. Genter, J.-P. Cautru, H. Fabriol, and P. Chèvremont, "Petrography of the granite massif from drill cutting analysis and well log interpretation in the geothermal HDR borehole GPK-1 (Soultz, Alsace, France)," in *Geothermal Energy in Europe: The Soultz Hot Dry Rock Project*, J. C. Bresee, Ed., pp. 1–29, Geothermal Science and Technology, Montreux, Switzerland, 1992.

[38] J.-M. Stussi, A. Cheilletz, J.-J. Royer, P. Chèvremont, and G. Féraud, "The hidden monzogranite of Soultz-sous-Forêts (Rhine Graben, France)," *Mineralogy, petrology and genesis. Géologie de la France*, vol. 1, pp. 45–64, 2002.

[39] C. Meller, A. Kontny, and T. Kohl, "Identification and characterization of hydrothermally altered zones in granite by combining synthetic clay content logs with magnetic mineralogical investigations of drilled rock cuttings," *Geophysical Journal International*, vol. 199, no. 1, pp. 465–479, 2014.

[40] C. Meller and B. Ledésert, "Is There a Link Between Mineralogy, Petrophysics, and the Hydraulic and Seismic Behaviors of the Soultz-sous-Forêts Granite During Stimulation? A Review and Reinterpretation of Petro-Hydromechanical Data Toward a Better Understanding of Induced Seismicity and Fluid Flow," *Journal of Geophysical Research: Solid Earth*, vol. 122, no. 12, pp. 9755–9774, 2017.

[41] J. Sausse, M. Fourar, and A. Genter, "Permeability and alteration within the Soultz granite inferred from geophysical and flow log analysis," *Geothermics*, vol. 35, no. 5-6, pp. 544–560, 2006.

[42] A. Genter, C. Castaing, C. Dezayes, H. Tenzer, H. Traineau, and T. Villemin, "Comparative analysis of direct (core) and indirect (borehole imaging tools) collection of fracture data in the hot dry rock Soultz reservoir (France)," *Journal of Geophysical Research: Solid Earth*, vol. 102, no. B7, pp. 15419–15431, 1997.

[43] A. Genter, H. Traineau, and D. Artignan, *Synthesis of Geological and Geophysical Data at Soultz-sous-Forêts (France)*, BRGM, Orléans, France, 1997.

[44] R. L. Hébert, B. Ledésert, D. Bartier, C. Dezayes, A. Genter, and C. Grall, "The Enhanced Geothermal System of Soultz-sous-Forêts: A study of the relationships between fracture zones and calcite content," *Journal of Volcanology and Geothermal Research*, vol. 196, no. 1-2, pp. 126–133, 2010.

[45] B. Ledésert, R. L. Hébert, C. Grall et al., "Calcimetry as a useful tool for a better knowledge of flow pathways in the Soultz-sous-Forêts Enhanced Geothermal System," *Journal of Volcanology and Geothermal Research*, vol. 181, no. 1-2, pp. 106–114, 2009.

[46] S. Nishimoto and H. Yoshida, "Hydrothermal alteration of deep fractured granite: effects of dissolution and precipitation," *Lithos*, vol. 115, no. 1-4, pp. 153–162, 2010.

[47] B. Jacquemont, "Etude des interactions eaux-roches dans le granite de Soultz-sous-Forêts. Quantification et modélisation des transferts de matière par les fluides," (PhD). Université de Strasbourg, France, 2002.

[48] G. L. Hunt and J. W. Salisbury, "Visible and near infrared spectra of minerals and rocks: I. Silictae minerals," *Modern Geology*, vol. 1, pp. 283–300, 1970.

[49] B. Hébert, *Approche quantitative par spectrométrie Vis-NIR des minéraux argileux et uranifères dans les sables du gisement de Tortkuduk, Kazakhstan*, Université de Poitiers, Poitiers, 2018.

[50] B. H. Toby, "*R* factors in Rietveld analysis: how good is good enough?," *Powder Diffraction*, vol. 21, no. 1, pp. 67–70, 2006.

[51] J. Madejová, W. P. Gates, and S. Petit, "IR spectra of clay minerals," in *Developments in Clay Science*, pp. 107–149, Elsevier, 2017.

[52] S. Pontual, N. Merry, and P. Gamson, *G-Mex Vol.1, Spectral interpretation field manual*, Ausspec international Pty. Ltd., Kew, Victoria 3101, Australia, 1997.

[53] A. Genter, H. Traineau, C. Dezayes et al., "Fracture analysis and reservoir characterization of the granitic basement in the HDR Soultz Project (France)," *Geothermal Science and Technology*, vol. 4, pp. 189–214, 1995.

[54] J. H. Duckworth, "Spectroscopic quantitative analysis," in *Applied Spectroscopy: A Compact Reference for Practitioners*, Academic Press, 1998.

[55] G. W. Brindley and G. Brown, *Crystal Structures of Clay Minerals and Their X-Ray Identification*, Mineralogical Society of Great Britain and Ireland, 1980.

[56] C. A. Barton, M. D. Zoback, and D. Moos, "Fluid flow along potentially active faults in crystalline rock," *Geology*, vol. 23, no. 8, pp. 683–686, 1995.

[57] J. Bradford, J. McLennan, J. Moore et al., "Recent Developments at the Raft River Geothermal Field," in *Presented at the Thirty-Eighth Workshop on Geothermal Reservoir Engineering, Stanford University*, California, USA, 2013.

[58] N. C. Davatzes and S. H. Hickman, "Controls on Fault-Hosted Fluid Flow; Preliminary Results from the Coso Geothermal Field, CA," in *Presented at the Geothermal Resources Council Transactions, Geothermal Resources Council*, pp. 343–348, Davis, California, 2005.

[59] L. Aquilina, M. Brach, J. C. Foucher, A. De Las Heras, and G. Braibant, *Deepening of GPK-1 HDR borehole 2000-3600m (Soultz-sous-Forêts, France), geochemical monitoring of drilling fluids (open file no. R36619)*, BRGM, Orléans, France, 1993.

[60] F.-D. Vuataz, M. Brach, A. Criaud, and C. Fouillac, "Geochemical monitoring of drilling fluids: a powerful tool to forecast and detect formation waters," *SPE Formation Evaluation*, vol. 5, no. 2, pp. 177–184, 1990.

[61] C. Gallé, "Neutron porosity logging and core porosity measurements in the Beauvoir granite, Massif Central Range, France," *Journal of Applied Geophysics*, vol. 32, no. 2-3, pp. 125–137, 1994.

[62] L. Lévy, B. Gibert, F. Sigmundsson et al., "The role of smectites in the electrical conductivity of active hydrothermal systems: electrical properties of core samples from Krafla volcano, Iceland," *Geophysical Journal International*, vol. 215, no. 3, pp. 1558–1582, 2018.

[63] B. I. Anderson, *Modeling and inversion methods for the interpretation of resistivity logging tool response*, Technische Universiteit Delft, Netherlands, 2001.

[64] O. Serra, *Fundamentals of Well-Log Interpretation*, Elsevier, Ed., ELF Aquitaine, Pau, France, 1984.

[65] Schlumberger, "HRLA High-Resolution Laterolog Array | Schlumberger [WWW Document]," Schlumberger, 2018, March 2018, https://www.slb.com/services/characterization/petrophysics/wireline/legacy_services/high_res_array.aspx.

[66] B. Sanjuan, R. Millot, C. Innocent, C. Dezayes, J. Scheiber, and M. Brach, "Major geochemical characteristics of geothermal brines from the Upper Rhine Graben granitic basement with constraints on temperature and circulation," *Chemical Geology*, vol. 428, pp. 27–47, 2016.

[67] R. Jung, "Hydraulic fracturing and hydraulic testing in the granitic section of borehole GPK-1, Soultz-sous-Forêts," in *Geothermal Energy in Europe, The Soultz Hot Dry Rock Project*, vol. 3, pp. 149–198, Geothermal Science and Technology, 1992.

[68] R. Schellschmidt and R. Schulz, "Hydrogeothermic studies in the Hot Dry Rock Project at Soultz-sous-Forêts," in *Geothermal Energy in Europe: The Soultz Hot Dry Rock Project*, vol. 3, pp. 217–238, Geothermal Science and Technology, 1992.

[69] C. Glaas, J. Vidal, P. Patrier, D. Beaufort, and A. Genter, "Contribution of SWIR to the Clay Signature of Permeable Fracture Zones in the Granitic Basement. Overview of Soultz and Rittershoffen wells," in *Presented at the European Geothermal Congress*, p. 11, Den Haag, The Netherlands, 2019.

[70] K. F. Evans, A. Genter, and J. Sausse, "Permeability creation and damage due to massive fluid injections into granite at 3.5 km at Soultz: 1. Borehole observations," *Journal of Geophysical Research*, vol. 110, no. B4, 2005.

[71] J. S. Caine, J. P. Evans, and C. B. Forster, "Fault zone architecture and permeability structure," *Geology*, vol. 24, no. 11, pp. 1025–1028, 1996.

[72] A. Richard, É. Gillot, V. Maurer, N. Cuenot, and J. Klee, "Upper Rhine Graben: The Largest Exploration by 3D Seismic Reflection," in *Presented at the European Geothermal Congress*, Den Haag, Netherlands, 2019.

Geofluids Journal

Supporting information for

How Do Secondary Minerals in Granite Help Distinguish Paleo- from Present-Day Permeable Fracture Zones? Joint Interpretation of SWIR Spectroscopy and Geophysical Logs in the Geothermal Wells of Northern Alsace

Carole Glaas[1,2,3], Jeanne Vidal[2,4], Patricia Patrier[3], Jean-François Girard[1], Daniel Beaufort[3], Sabine Petit[3], Albert Genter[2]

[1]University of Strasbourg, CNRS, UMR 7516 IPGS, 5 Rue René Descartes, 67084 Strasbourg Cedex, France
[2]ES-Géothermie, Bat Le Belem 5 rue de Lisbonne, 67300 Schiltigheim, France
[3]University of Poitiers, CNRS UMR 7285 IC2MP, HydrASA, Bat B8 rue Albert Turpain, TSA51106, F-86073 Poitiers Cedex 9, France
[4]University of Chile, FCFM, Dept. of Geology, Andean Geothermal Center of Excellence (CEGA), Plaza Ercilla 803, Santiago, Chile

Content of this file

Text S1, S2, S3 and captions of Figures S1, S2 and S3.

Introduction

This supporting information provides details on the SWIR results acquired in both GRT-2 and GPK-1 wells like the intra-sample variability and comparison between manual fit and automatic fit with the TSS software.

Text S1 and S2

For both GRT-2 and GPK-1 wells the intra-sample variability of the granite cuttings was tested. As each cuttings bag represents sections of drilled rocks (see section 3.1.1.) and as the cuttings could not be homogeneously mixed in the bag, several measurements were carried out on the same cuttings bag. In the GRT-2 well 10 measurements were done on the same cuttings bag (Figure S1) whereas only 5 measurements were done in the GPK-1 well (Figure S2) because of a lower amount of cuttings available. Error bounds were then calculated for each cuttings bag in order to observe if the range of variation is not exceeding the scattering of the data. In both wells, we can observe that the variability is low in unaltered granite and higher in the hydrothermally altered granite. Also, the variability observed in the GRT-2 well is higher

than in the GPK-1 well. These differences in both wells could be due to the heterogeneity of the mineralogy.

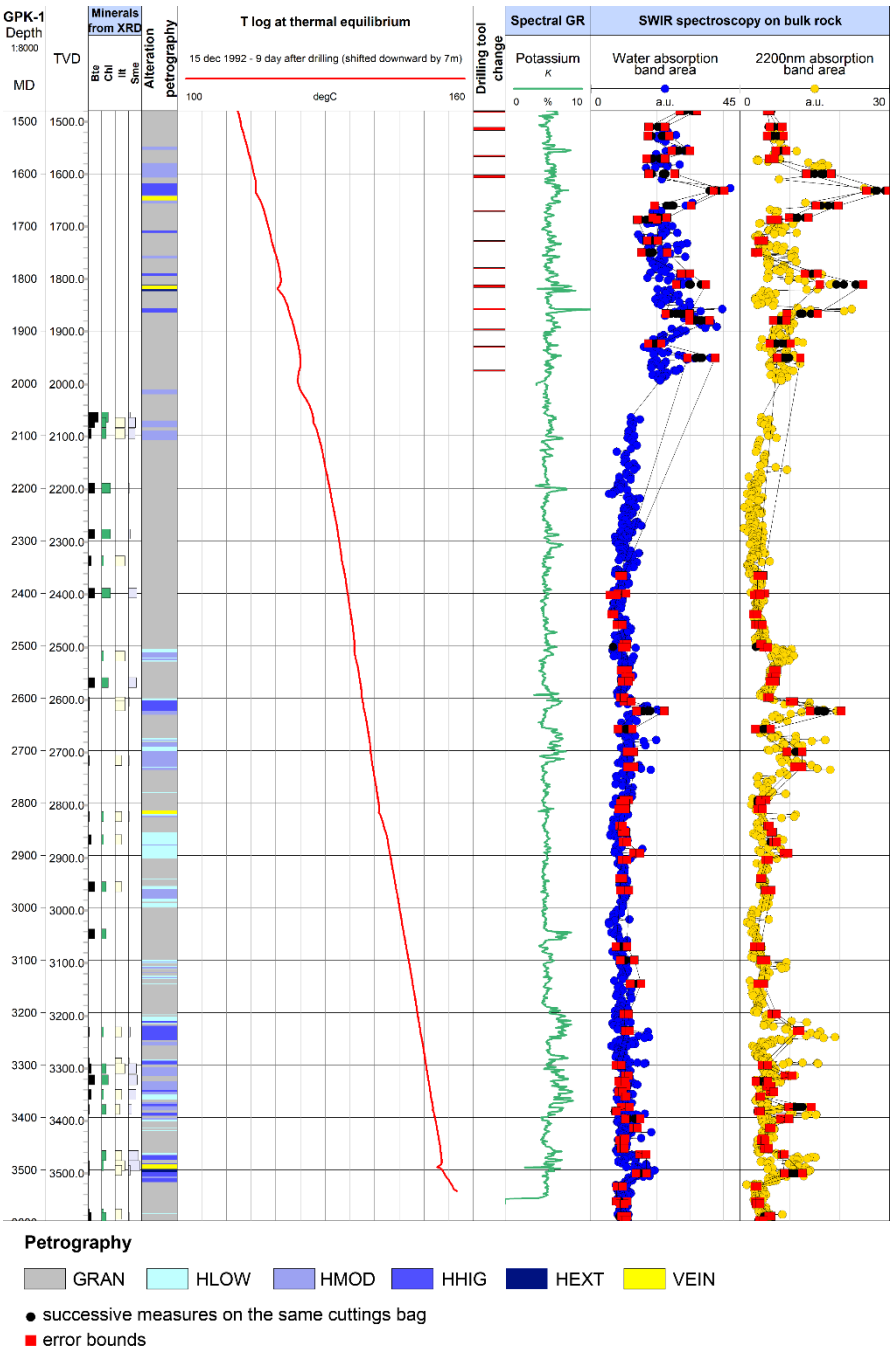

Figure S1: Composite log of the GPK-1 well presenting the secondary minerals, the petrographical log built from the mineralogical observations, the temperature log, the spectral K-GR log and the SWIR results. The successive measurements realized for each cuttings bag are represented by black full circles and the error bounds calculated from these successive measurements are represented by the distance between red squares for each cuttings bag.

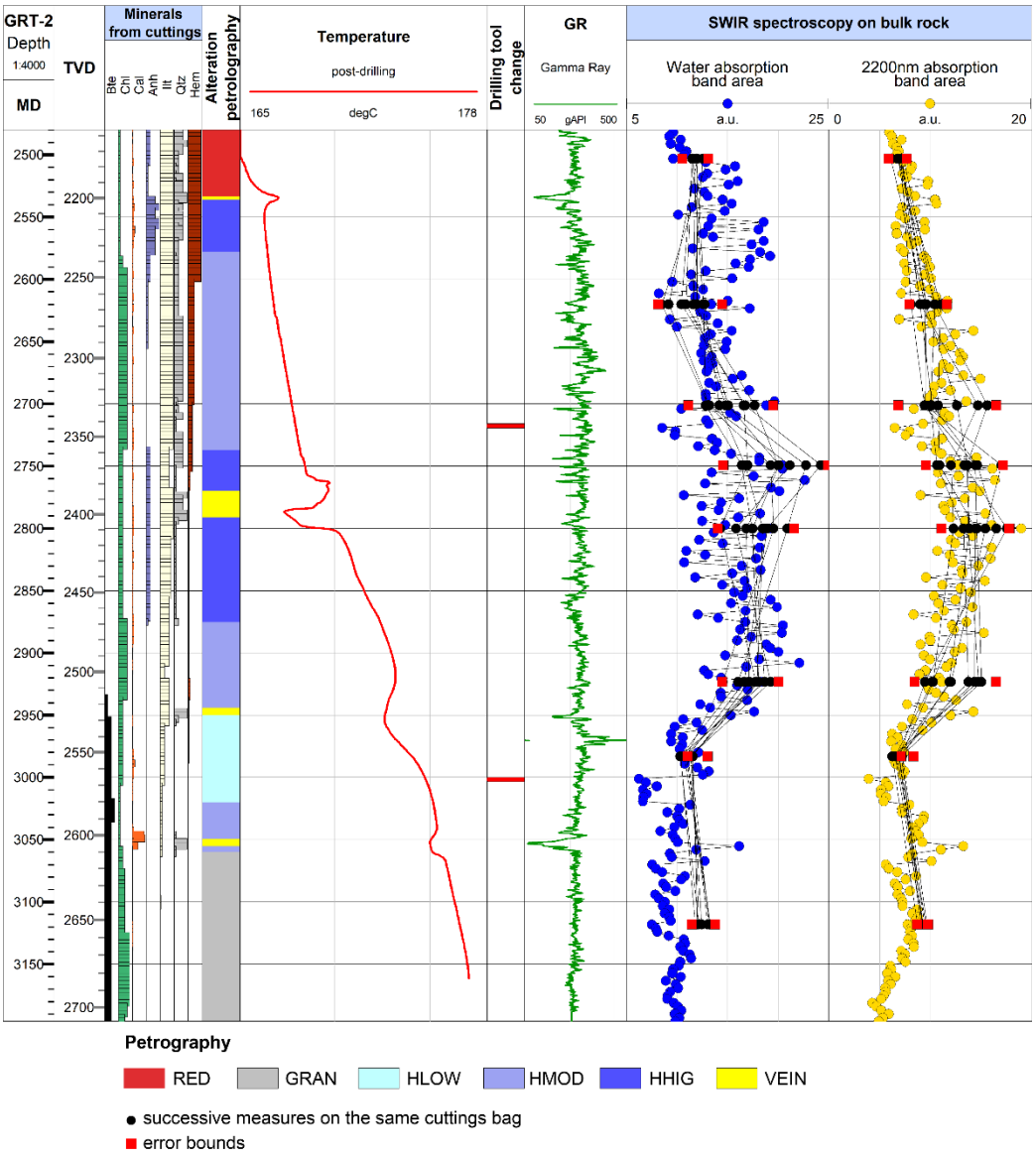

Figure S2: Composite log of the GRT-2 well presenting the secondary minerals, the petrographical log built from the mineralogical observations, the temperature log, the GR log and the SWIR results. The successive measurements realized for each cuttings bag are represented by black full circles and the error bounds calculated from these successive measurements are represented by the distance between red squares for each cuttings bag.

Text S3

For the GRT-2 well, position and half width at half maximum (HWHM) were locked for each simulation profile. However, different sets of position and HWHM were used. The simulation profiles were accepted with a weighted profile R-factor (Rwp) lower than 0.05. For the GPK-1 well, with regard to the huge amount of profiles calculated (1190), position and HWMH were free fitted by TSS for each simulation profile. The areas of the water absorption band and the 2200 nm absorption band were also fitted manually

for some profiles to compare if there is a significant deviation of the area with the free fitting. Results showed that there was no significant change in the area between profiles fitted manually or free-fitted by TSS for the GPK-1 well (Figure S3).

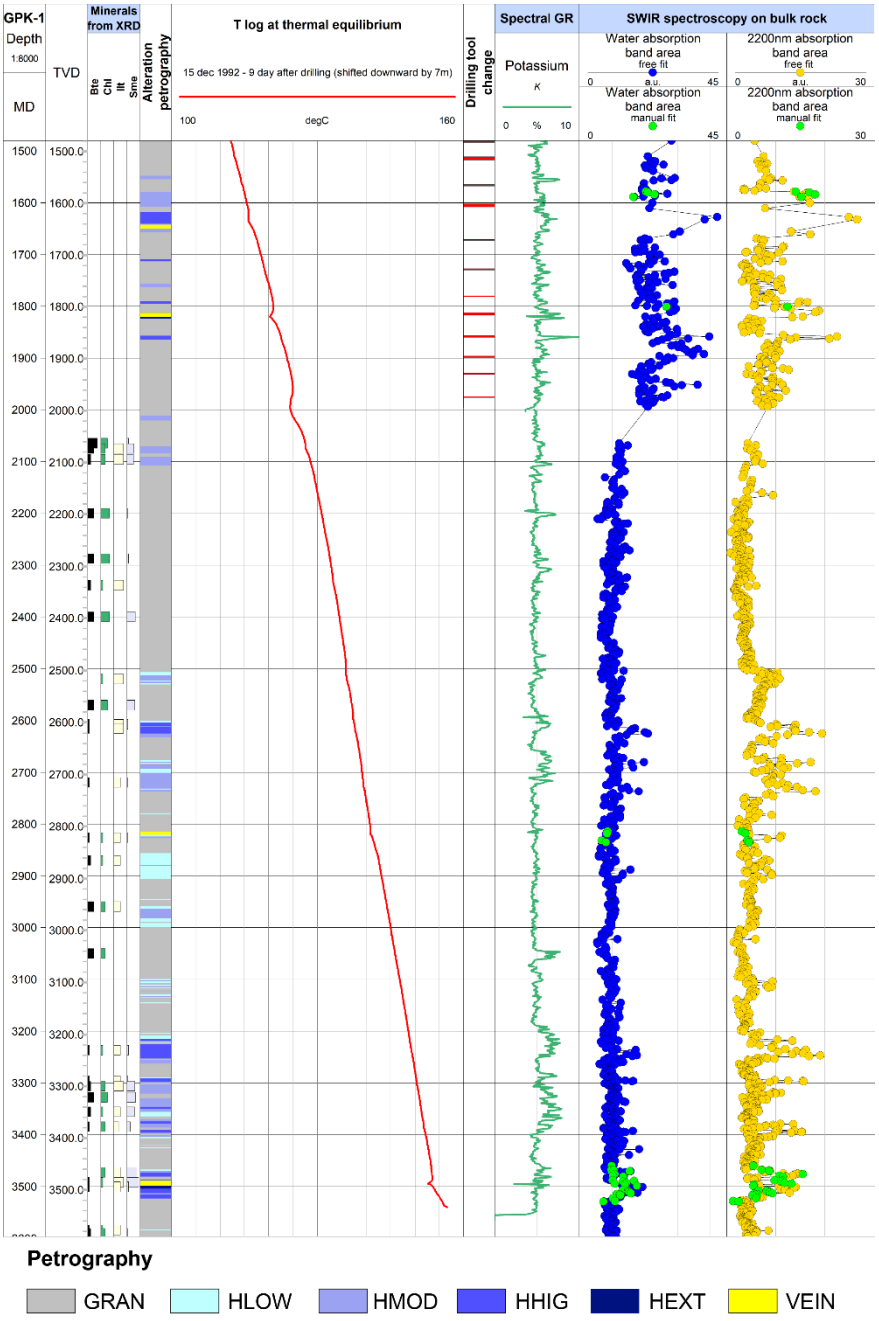

Figure S3: Composite log of the GPK-1 well presenting the secondary minerals, the petrographical log built from the mineralogical observations, the temperature log, the spectral K-GR log and the SWIR results that were free-fitted with the TSS software (blue and yellow full circles for water and 2200 nm absorption band areas, respectively). The light green full circles represent the SWIR results manually fitted.